Three-dimensional imaging

Living cells were stained with 20 nM MitoTracker Red and 500 nM SYTO 16 (Molecular Probes) for 30 minutes at 37°C. The cells were scanned using 0.4 μm sections with the confocal laser-scanning microscope. Three-dimensional (3D) views were reconstructed with Fluoview software (Olympus) and volumes of the nucleus and mitochondria were calculated by summing fluorescent areas from each section using the NIH Image program (developed at the US National Institutes of Health and available on http://rsb.info.nih.gov./nih-image).

Separation of phospholipids

Total lipids were extracted from transfectants using methanol/chloroform as described (Folch et al., 1957). For the separation and detection of phospholipids, total lipids were injected into a HPLC system (model 616; Waters) fitted with a Wakosil 5Sil column (Wako, Tokyo, Japan). The mobile phase was a mixture of n-hexan, isopropanol, ethanol, acetic acid and 25 mM potassium phosphate buffer (pH 7.0) (146:282.5:50:0.3:31; v/v/v/v/v). The flow rate was 1 ml/minute. The elution of phospholipids was monitored at 205 nm with the UV detector (SPD-10A; Shimadzu). Retention times and quantities of phospholipids were determined using a phospholipid kit (Doosan Serdary Research Laboratory) as a standard.

Results

Cloning of genes that respond to a depletion of mtDNA

To identify nuclear genes that respond to a depletion of mtDNA, we screened for mRNA whose expression increased in cells lacking mtDNA using the differential mRNA display technique (Liang and Pardee, 1992) (Fig. 1A) by comparing mRNA populations in a HeLa derivative lacking mtDNA (EB8) (Hayashi et al., 1991) and control cybrid cells (Ft2-11) (Hayashi et al., 1994). Bands 1 and 2, which were stronger in EB8 than in Ft2-11 (Fig. 1A), were found to correspond to the apurinic/apyrimidinic endonuclease I (APE1/HAP1) (Demple et al., 1991) and DNA ligase III genes (Wei et al., 1995), respectively. The products of these genes are localized in mitochondria and involved in mtDNA repair (Kang and Hamasaki, 2002).

DNA sequencing distinguished the gene corresponding to the third band in Fig. 1A from the genes which have been so far identified to be involved in mitochondrial biogenesis, gene expression and metabolism. The full-length cDNA was isolated from a human brain cDNA library (Gibco-BRL) to confirm the increase in its mRNA (Fig. 1B,C) and its product (Fig. 1D,E) by northern and western blotting, respectively. We named this gene *MIDAS* (mitochondrial DNA absence sensitive factor), because the gene product was expressed in response to mtDNA depletion. Interestingly, the nucleotide sequence was identical to *GPP34* (GenBank accession no. AJ296152) whose product has been identified as a Golgi protein of unknown function(s) (Bell et al., 2001). In addition, MIDAS/GPP34 contains an isoform named GPP34R (GenBank accession no. AJ296153), which is highly homologous with MIDAS/GPP34 (supplementary material Fig. S1). In fact, GPP34R was expressed in cells with the HeLa nucleus as detected by northern blotting (supplementary material Fig. S2A). Interestingly, GPP34R was also expressed more abundantly in EB8 than in Ft2-11 (supplementary material Fig. S2A). The relative amount of GPP34R mRNA was semi-quantified by the TaqMan probe method and found to be less than 2% of that in

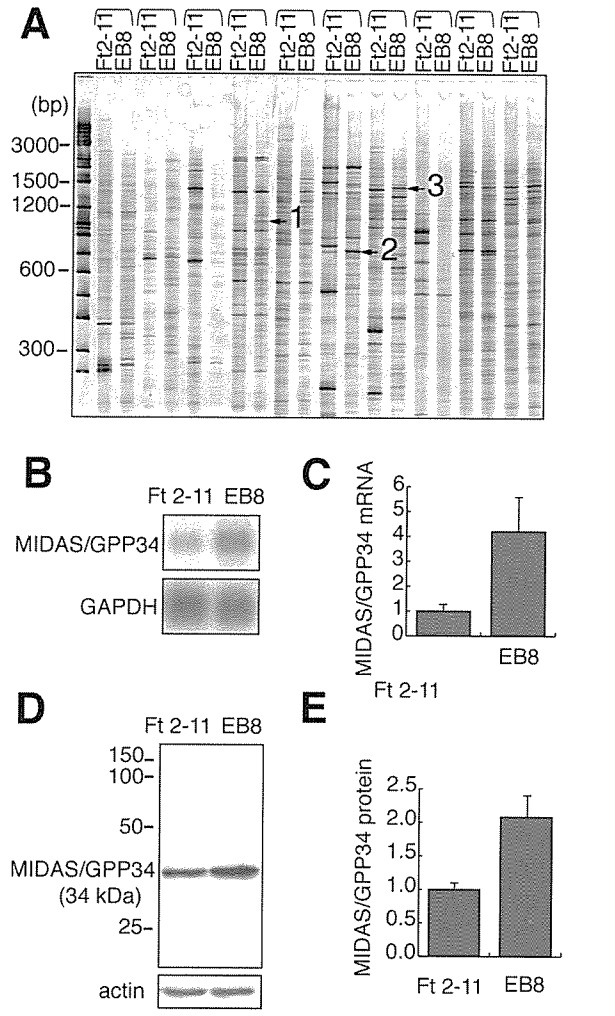

Fig. 1. Enhanced expression of MIDAS/GPP34 in EB8 (mtDNA-free HeLa cells). (A) Comparison of mRNA obtained from Ft2-11 with that from EB8 by differential display. EB8 lacks mtDNA whereas Ft2-11 is derived from EB8 but has wild-type mitochondria. Ten sets of arbitrarily primed PCR products were subjected to 5% PAGE. Three bands indicated by arrows were cloned and sequenced. Bands 1, 2 and 3 corresponded to apurinic/apyrimidinic endonuclease I, DNA ligase III and MIDAS/GPP34, respectively. (B) Northern blots of total RNA extracted from Ft2-11 and EB8 were hybridized with *GPP34*- and *GAPDH* (glyceraldehyde-3-phosphate dehydrogenase)-specific probes. (C) *GPP34* mRNA levels normalized to *GAPDH* levels based on the mean values±s.d. for three sets of northern blotting experiments (vertical bars). (D) Western blotting of Ft2-11 and EB8. Whole-cell lysates were separated by 12% SDS-PAGE and transferred onto a PVDF membrane. MIDAS/GPP34 was immunostained with anti-MIDAS antibody. (E) The MIDAS/GPP34 protein normalized against actin. Mean values of three sets of experiments are shown with s.d. (vertical bars).

MIDAS/GPP34 (supplementary material Fig. S2B). Therefore, we focused on the function of MIDAS/GPP34.

Specific expression of MIDAS/GPP34 in muscle fibers with abnormal mitochondria

Mitochondria accumulate in response to their own dysfunction

in mitochondrial diseases (Schon, 2000; Wallace, 1999). We examined the expression of MIDAS/GPP34 in muscle fibers of patients with mitochondrial diseases. Large deletions and a point mutation in the $tRNA^{Leu(UUR)}$ gene of mtDNA are responsible for the subgroups of mitochondrial diseases, CPEO (chronic progressive external ophthalmopelia) (Holt et al., 1988; Shoubridge et al., 1990) and MELAS (mitochondrial myopathy, encephalopathy, lactic acidosis and stroke-like episodes) (Goto et al., 1990; Kobayashi et al., 1990; Kobayashi et al., 1991), respectively. Accumulations of abnormal mitochondria are detected as ragged-red fibers and high succinate dehydrogenase (SDH) fibers, with mutant mtDNA dominating in a mosaic manner (Engel and Cunningham, 1963; Hasegawa et al., 1991; Lightowlers et al., 1997).

Muscle sections from a normal subject and patients with CPEO or MELAS were stained for activity of SDH and cytochrome c oxidase (COX) and with anti-MIDAS antibody. No MIDAS-positive fibers were detected in normal muscle, whereas MIDAS-positive fibers were detected in the muscle sections of affected patients (Fig. 2). The amount of MIDAS in the positive muscles increased approximately twofold compared to those in the negative muscles. It is noted that MIDAS was more abundant specifically in fibers with an SDH^{++}/COX^{-} phenotype (Fig. 2, asterisks). Thus, MIDAS is expressed in response to mitochondrial dysfunction in muscle with mitochondrial diseases.

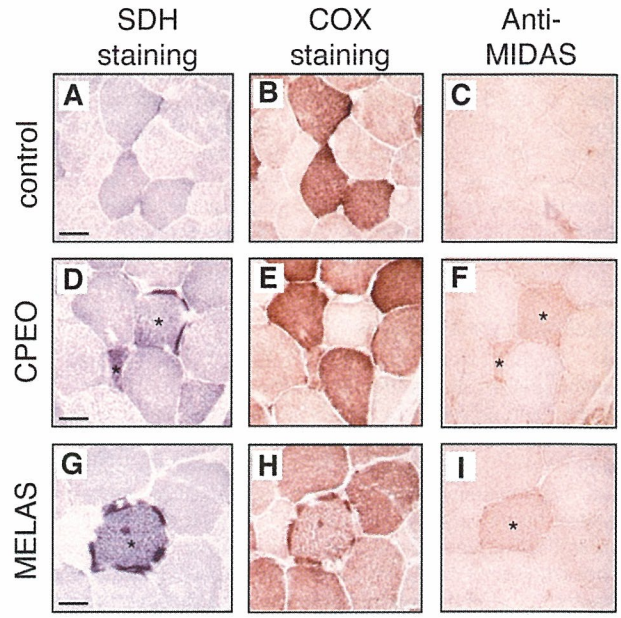

Fig. 2. Expression of MIDAS/GPP34 in SDH^{++}/COX^{-} muscle cells of patients with mitochondrial diseases. Biopsy samples were obtained from the biceps brachii muscle. Activities of SDH and COX were visualized histochemically and the expression of MIDAS/GPP34 was detected with anti-MIDAS antibody. (A-C) Control muscle without mitochondrial disorder. (D-F) Muscle from a patient with CPEO who has a common deletion in mtDNA. (G-I) Muscle from a patient with MELAS who has a point mutation at nucleotide number 3243 in the $tRNA^{Leu(UUR)}$ gene. Asterisks indicate SDH^{++}/COX^{-} cells of patients with increased MIDAS/GPP34 expression. Bars, 50 μm.

Subcellular distribution of MIDAS/GPP34

GPP34 has been isolated as a Golgi peripheral membrane protein in a Golgi proteomics study (Bell et al., 2001). To verify the distribution of MIDAS in mitochondria, we immunostained HeLa cells with an affinity-purified polyclonal antibody against the MIDAS protein. Immunostaining of HeLa cells revealed that MIDAS mainly colocalized with MitoTracker Red (Fig. 3A). The mitochondrial localization was confirmed with another mitochondrial marker, Hsp60 (data not shown). With careful observation, we found MIDAS in an additional region, the perinuclear area, where MitoTracker Red was absent (Fig. 3A, merge; indicated by white arrowhead). This region corresponds to the Golgi apparatus, as judged by immunostaining with anti-p230 (the *trans*-Golgi membrane protein) (Erlich et al., 1996) antibody (Fig. 3B). These results suggest that a majority of MIDAS/GPP34 localizes to mitochondria, but some is distributed in the Golgi apparatus.

This finding disagrees with the previous study on GPP34 showing that GPP34 is located in the Golgi apparatus, but not in mitochondria (Bell et al., 2001). This discrepancy could be due to a different fixation method prior to staining. In general, for immunostaining of cultured cells, the permeabilization of intramembranes with an organic solvent or detergent is essential for antibodies to penetrate the membranes of organelles (Zeller, 1998). In fact, under the same conditions as the published experiment (no permeabilization pretreatment), MIDAS did not show colocalization with mitochondria (Fig. 3D), being detected only in the Golgi apparatus (Fig. 3E). Moreover, several marker proteins were immunostained to confirm that the permeabilization pretreatment with acetate in cold ethanol is essential for detecting the mitochondrial proteins located internally. Without permeabilization pretreatment, cytosolic (Hsc70), mitochondrial outer membrane (Tom20) and *trans*-Golgi (p230) proteins were stained with each antibody (Fig. 3F), whereas the mitochondrial intermembrane space protein (cytochrome c) could not be detected (Fig. 3F). Alternatively, cytochrome c required an acetate/ethanol pretreatment for permeabilization as described in Materials and Methods to be detected (Fig. 3C). Moreover, a mitochondrial matrix protein (Hsp60) and an inner membrane protein (SDH70) were clearly stained only with the acetate/ethanol pretreatment (supplementary material Fig. S3). Therefore, the mitochondrial MIDAS/GPP34 protein is located inside mitochondria or embedded in the outer membrane. In addition, immunostaining with anti-KDEL, the signal peptide targeting the endoplasmic reticulum (ER) (Munro and Pelham, 1987), showed no localization of MIDAS/GPP34 to the ER (data not shown).

To further investigate the subcellular distribution of MIDAS, Myc-tagged constructs were generated. A gene corresponding to a Myc peptide was fused to the gene of the N-terminus (Myc-MIDAS) or C-terminus (MIDAS-Myc) of MIDAS. Fusion constructs were transfected into HeLa cells and the cells were allowed to express the protein for 16 hours. The transfected cells were immunostained with anti-Myc antibody. Myc-MIDAS was localized to the perinuclear area and colocalized with the p230 *trans*-Golgi (Fig. 3G). On the other hand, MIDAS-Myc was distributed in both mitochondria and Golgi as stained with anti-MIDAS antibody (Fig. 3H). This

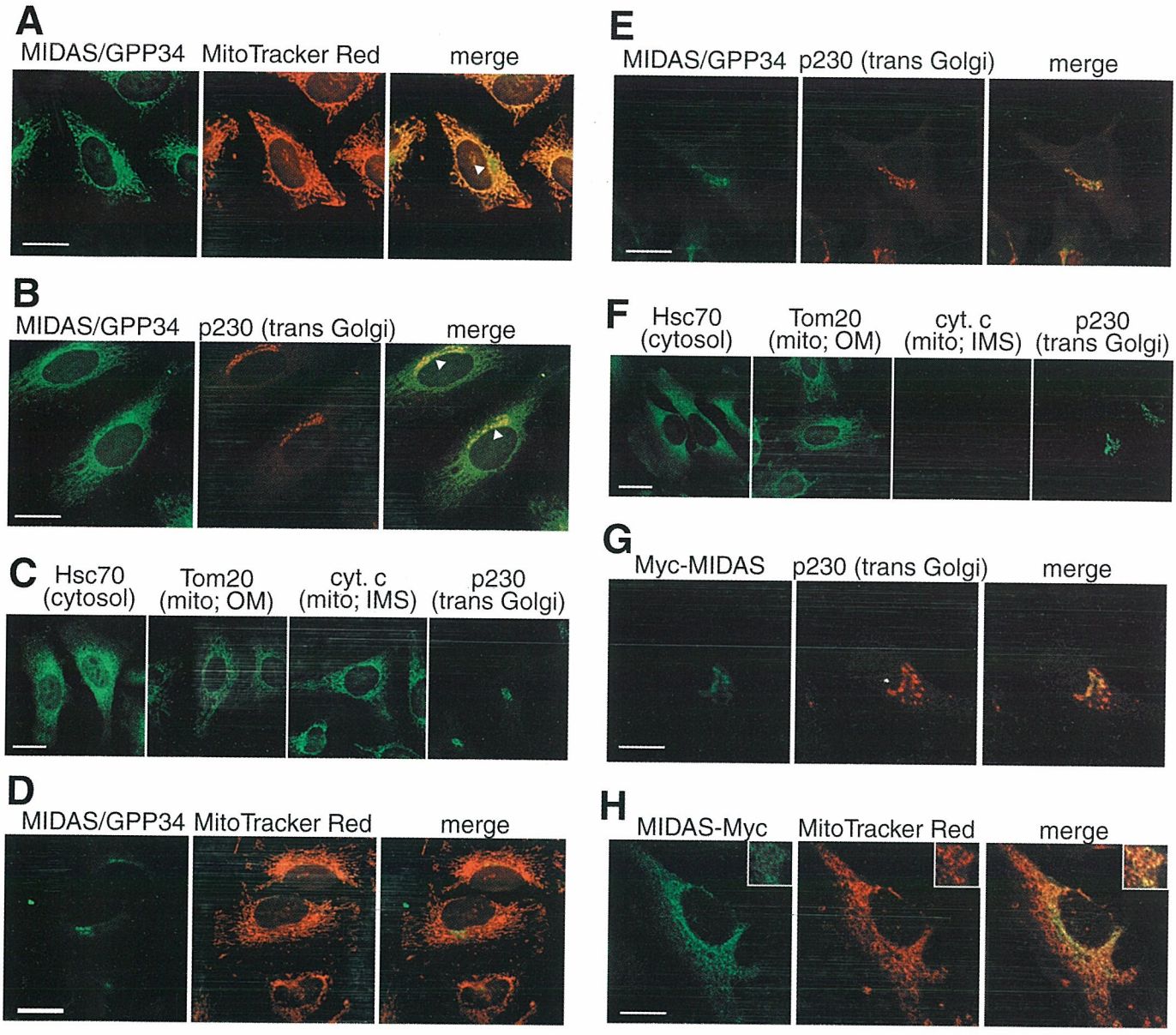

Fig. 3. Localization of MIDAS/GPP34 in mitochondria and the Golgi apparatus. (A-C) HeLa cells in culture were fixed, permeabilized with 5% acetic acid in ethanol and then immunostained with various antibodies. (A) MitoTracker Red (100 nM) was added as a mitochondrial indicator prior to fixation. MIDAS/GPP34 was detected with anti-MIDAS antibody. Arrowhead indicates where MIDAS/GPP34 is more abundant than mitochondria in a perinuclear area. (B) MIDAS/GPP34 and p230 (*trans*-Golgi) were double-stained immunochemically using different secondary antibodies. Arrowheads indicate where the perinuclear area was co-stained with both antibodies. (C) Hsc70 (cytosol), Tom20 (outer membrane of mitochondria), cytochrome c (cyt. c) (intermembrane space of mitochondria) and p230 (*trans*-Golgi) were detected with their respective antibodies. (D-F) HeLa cells in culture were fixed with 4% paraformaldehyde and 4% sucrose without treatment for permeabilization and immunostained with the same procedure as in (A-C). (G,H) Localization of Myc-tagged MIDAS. A Myc tag was fused to the N-terminus (G) or C-terminus (H) of MIDAS. Fusion constructs were transfected into HeLa cells and cells were allowed to express protein for 16 hours. Cells were stained with anti-Myc, anti-p230 antibodies or MitoTracker Red with the same procedure as in (A-C). Bars, 20 μm.

finding suggests that MIDAS potentially localizes to both mitochondria and the Golgi apparatus.

To demonstrate the subcellular distribution of MIDAS, organelles were sub-fractionated with a Nycodenz gradient. HeLa cells were homogenized, the homogenate was fractionated with a 7-35% density gradient and the distribution of MIDAS was examined by western blotting (Fig. 4A). The majority of MIDAS was detected in the mitochondrial fractions (with Tom20 and Hsp60) and small portions were fractionated with the Golgi (with a Golgi marker, Syntaxin6) and cytosol. Relative amounts of MIDAS distributed in the fractions for mitochondria (fractions 13-17), Golgi (fractions 6-12) and cytosol (fractions 1-5) were 0.75, 0.19 and 0.06, respectively, as judged by the densities of total bands.

To determine the sub-mitochondrial distribution of MIDAS, the mitochondria purified from HeLa cells were treated with

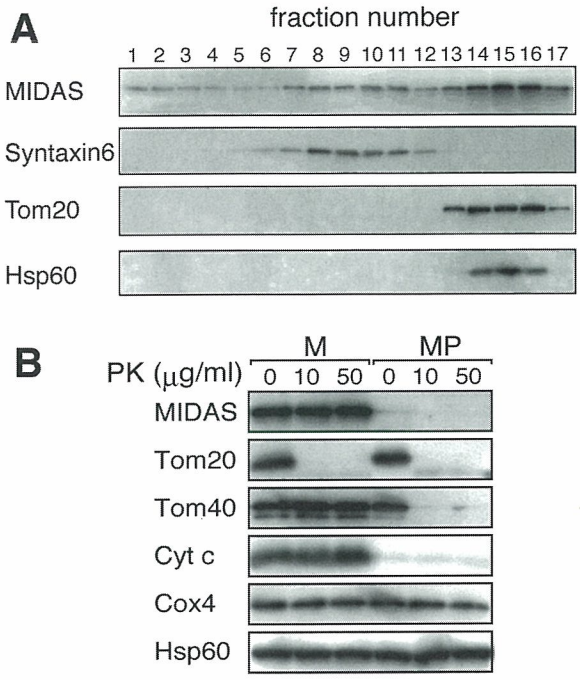

Fig. 4. Localization of MIDAS/GPP34 in the mitochondrial intermembrane space. (A) Fractionation of organelles of HeLa cells in 7-35% (w/v) preformed density gradients. The distribution of MIDAS was detected by western blotting. Syntaxin6 was used for a Golgi marker. Tom20 and Hsp60 were used for mitochondrial markers. (B) Mitoplasts were obtained from the mitochondrial fraction (fraction 15 in A) by osmotic disruption of the outer membrane. The mitochondria (M; lanes 1-3) and the mitoplasts (MP; lanes 4-6) were treated with proteinase K (PK; 10 μg/ml or 50 μg/ml). Mitochondrial sub-fractions were monitored by western blotting with antibodies directed against Tom20 (an outer membrane protein; most of which is exposed outside mitochondria), Tom40 (an outer membrane protein), cytochrome c (cyt c) (an intermembrane space protein), Cox4 (an inner membrane protein) and Hsp60 (a matrix space protein).

proteinase K. Both Tom40 and Tom20 are embedded in the outer membrane, whereas Tom20 is exposed to the outside of mitochondria (Pfanner and Geissler, 2001). Tom20 was easily digested with 10 μg/ml proteinase K, whereas Tom40 and MIDAS were resistant (Fig. 4B, M). On the other hand, when mitochondria were converted to mitoplasts, MIDAS disappeared (Fig. 4B, MP) even without proteinase K, as cytochrome c disappeared. From these results, it was concluded that the majority of MIDAS protein is located in the intermembrane space of mitochondria, with a small fraction present in the Golgi apparatus.

Mitochondrial accumulation without swelling by MIDAS

To determine the function of MIDAS in mitochondria, HeLa cells were transfected with *MIDAS* cDNA under the control of the CMV promoter. We could isolate transfectants constitutively expressing MIDAS at low levels (1.5- to 2-fold increase) (Fig. 5A, upper left panel, CMV-MIDAS3 and CMV-MIDAS9). Cells transiently transfected with a higher level of MIDAS could undergo cell division once or twice but did not survive for a week (data not shown), suggesting that overproduction of MIDAS prevents cell growth. To downregulate MIDAS, we then constructed HeLa transfectants expressing siRNA (small interfering RNA) of *MIDAS* to inhibit the endogenous MIDAS expression (Fig. 5A, upper right panel).

These transfectants were stained with MitoTracker Red to visualize mitochondria, in a short period to monitor the membrane potential of mitochondria. Even low levels of additional MIDAS expression caused a change in the distribution of mitochondria. The mitochondria in a *MIDAS* transfectant CMV-MIDAS3 were concentrated around the nucleus (Fig. 5B, second panel), whereas those in the control transfectants remained dispersed (Fig. 5B, first panel).

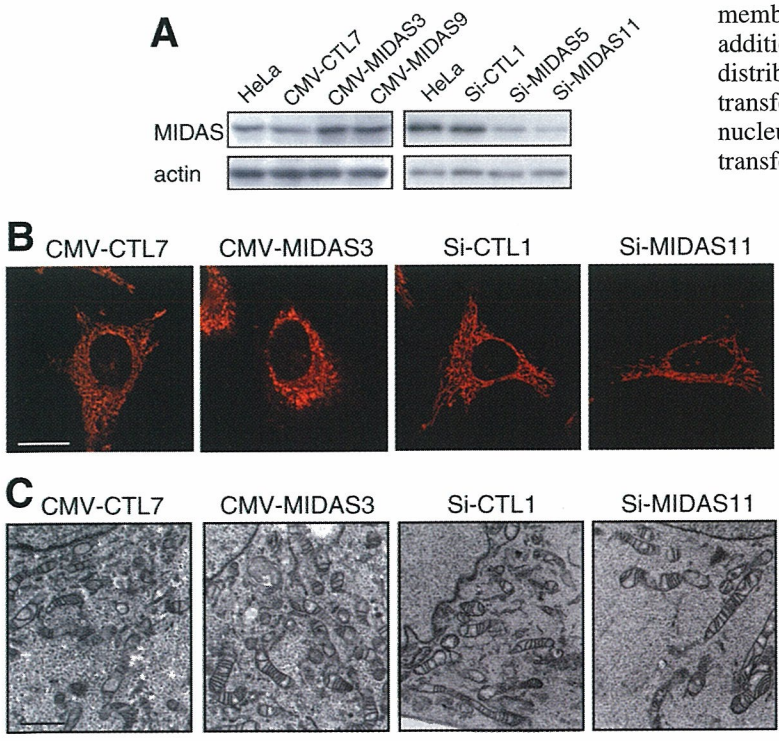

Fig. 5. The increased or decreased mass of intact mitochondria related to MIDAS concentration. (A) CMV-CTL7 and Si-CTL1 are stable control transfectants derived from HeLa cells. Although CMV-MIDAS3 and CMV-MIDAS9 are stable *MIDAS* transfectants under the control of the CMV promoter. Si-MIDAS5 and Si-MIDAS11 were transfectants expressing siRNA of *MIDAS* constitutively. Total cell lysate was extracted from each transfectant cell line and subjected to western blotting with anti-MIDAS and anti-actin antibodies. (B) Control (CMV-CTL7 and Si-CTL1), *MIDAS* transfectants (CMV-MIDAS3) and siRNA *MIDAS* transfectants (Si-MIDAS11) were stained with MitoTracker Red and visualized by confocal scanning laser microscopy. (C) Electron micrographs (×8000) of mitochondria in the transfectants. Bar, 20 μm (B); 1 μm (C).

Moreover, mitochondria in the MIDAS-expressing transfectants were stained more strongly than those in the control cells. Another transfectant clone CMV-MIDAS9 showed the same results (data not shown).

The mitochondria in a siRNA *MIDAS* transfectant, Si-MIDAS11, were dispersed similarly to those in the control transfectant (Si-CTL1) but were less intensely stained (Fig. 5B, third and fourth panels). Another siRNA *MIDAS* transfectant, clone Si-MIDAS5, showed the same results (data not shown).

Electron microscopy showed that mitochondria in the *MIDAS* transfectant were somewhat larger with no marked change in morphology and were neither pathologically swollen nor had lost the cristae structure (Fig. 5C, second panel). In addition, the *MIDAS* transfectants increased the number of mitochondria, whereas the siRNA-transfectants decreased the number of mitochondria (Fig. 5C, fourth panel). These photographs suggest that the number of mitochondria around the nucleus was increased by MIDAS.

Increase in total mitochondrial mass by MIDAS

To quantify the accumulation of mitochondria suggested above, cells were stained with two mitochondria-specific dyes, MitoTracker Red and MitoTracker Green and subjected to flow cytometric analysis (Fig. 6A-C). There was no significant difference in forward scatter among any of the cells examined (FS in Fig. 6C), indicating that MIDAS does not have any influence on cell size, regardless of the up- or downregulation of its expression. MitoTracker Green, but not MitoTracker Red, binds to mitochondria in a membrane-potential-independent manner and fluoresces only in the lipid environment of mitochondria. Fluorescent intensity in green (MitoTracker Green) was measured to estimate overall mitochondrial mass, whereas fluorescent intensity in red (MitoTracker Red) was measured to assess the content of energized mitochondria. The intensities in green and red significantly increased in MIDAS-expressing transfectants (CMV-MIDAS) (Fig. 6A,C). On the other hand, the green and red intensities decreased in the MIDAS downregulated transfectants (Si-MIDAS) (Fig. 6B,C). Quantitative analysis showed that the fluorescent intensities increased 1.5- to 2-fold in the MIDAS-expressing transfectants and decreased to 60-70% in the downregulated transfectants, compared to the control cells, respectively (Fig. 6C). The ratio of the intensity in red to the intensity in green was the same in all the cells examined, indicating that MIDAS does not exert any influence on the membrane potential. To confirm the increase in mitochondria, we stained transfectants with an additional fluorescent dye, TMRM (tetra-methyl-rhodamine methyl ester) specific to mitochondria and obtained a consistent result (supplementary material Fig. S4).

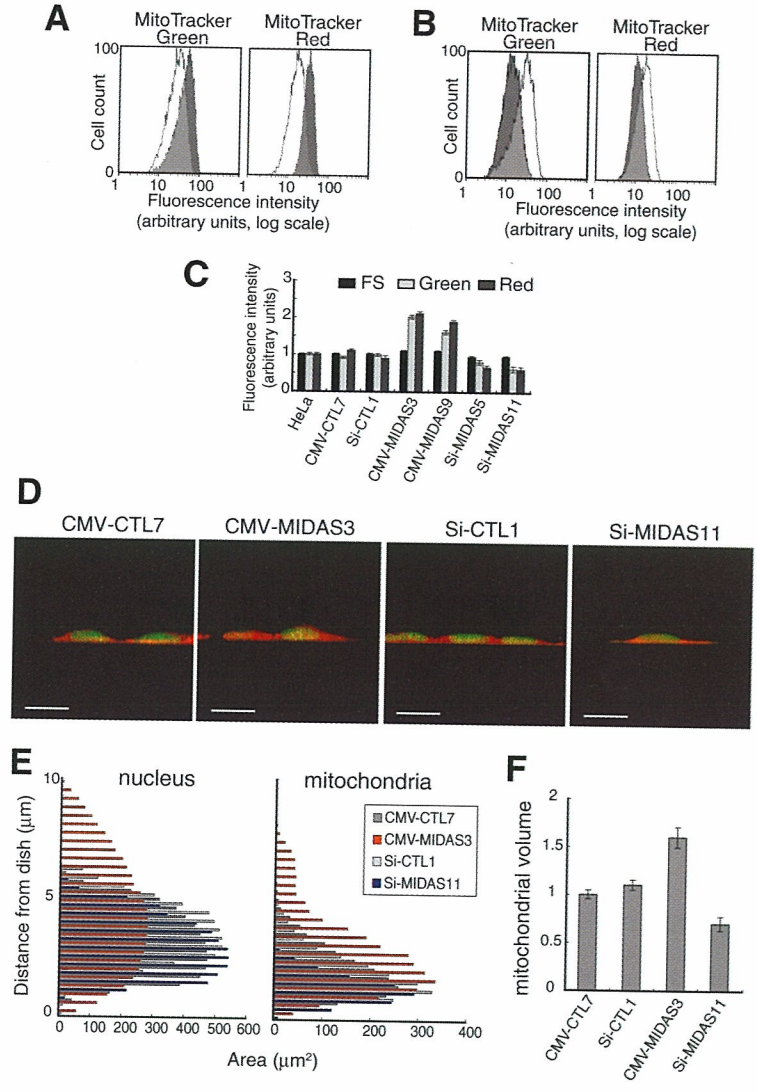

Fig. 6. Changes in mitochondrial mass with MIDAS. (A) Flow cytometric profiles of the fluorescence of dyes specific to mitochondria in CMV-CTL7 (white) and CMV-MIDAS3 (gray). Living transfectants were stained with MitoTracker Green (left) or MitoTracker Red (right) and analyzed with a flow cytometer. (B) Flow cytometric analysis performed with Si-CTL1 (white) and Si-MIDAS11 (gray) cells as described in A. (C) Fluorescence intensity (MitoTracker Green and MitoTracker Red) as well as forward scatter (FS) of HeLa cells and transfectants as quantified by flow cytometry. Values are the mean±s.d. (D) The mitochondria and nucleus in control transfectants (CMV-CTL7 and Si-CTL1), *MIDAS* transfectants (CMV-MIDAS3) and siRNA *MIDAS* transfectants (Si-MIDAS11) were stained with MitoTracker Red and SYTO 16 (green), respectively and scanned by confocal laser microscopy in each 0.4 μm section. Then the side view of a three-dimensional image was reconstructed with Fluoview software. (E) Areas of the nucleus and mitochondria were measured for each section. (F) The total mass of mitochondria in the transfectants was calculated based on the values in E and normalized to that of nucleus. Data represent the mean±s.d. of three sets of experiments. Bars, 20 μm.

The increase in the fluorescence of MitoTracker Green strongly suggests a substantial increase in total mitochondrial mass caused by MIDAS. Therefore, we estimated total mitochondrial volume by three-dimensional reconstitution of cells. Cells were stained with MitoTracker Red (red) for mitochondria and SYTO 16 (green) for the nucleus, respectively. The cells were scanned from bottom to top at intervals of 0.4 μm and each image was analyzed to measure the areas stained with MitoTraker Red and SYTO 16,

separately (Fig. 6E). Interestingly, the side view of the reconstituted three-dimensional image showed that mitochondria in the transfectants expressing MIDAS accumulated at the periphery of the nucleus (Fig. 6D, second panel), whereas in the downregulated transfectants, mitochondria appeared to be decreased in number (Fig. 6D, fourth panel). It is noted that there was no difference in nuclear volume between cells, although their three-dimensional shapes were different. On average, mitochondria occupied 22%, 35% and 15% of the total cytoplasm in controls, MIDAS-expressing transfectants and siRNA transfectants, respectively. The total volume of mitochondria was increased 1.6-fold by the MIDAS expression and decreased 0.75-fold by the downregulation of MIDAS, when normalized to that of the nucleus (Fig. 6F). Thus, the total mitochondrial mass varied more than 2.3-fold with the up- and downregulation of MIDAS. These results clearly indicate that MIDAS regulates total mitochondrial mass.

Regulation of cardiolipin by MIDAS

Flow cytometric analysis using MitoTracker Green showed that mitochondrial lipids varied in a MIDAS-dependent manner. Furthermore, the analysis using the fluorescent dye NAO (nonyl acridine orange), which detects cardiolipin, a mitochondria-specific phospholipid, revealed that the amount of cardiolipin varied according to amount of MIDAS (supplementary material Fig. S5). To obtain direct evidence for an increase in mitochondrial lipids caused by MIDAS, we measured levels of cardiolipin by HPLC. Total lipids were extracted from each transfectant and separated by HPLC as described in the Materials and Methods (Fig. 7A). The peak of cardiolipin (CL) was found to increase in MIDAS-expressing transfectants, compared with control transfectants. In clear contrast, the CL peak decreased in the MIDAS downregulated transfectants. The relative amount of each phospholipid was quantified based on the HPLC peak (Fig. 7B). The results showed that the amount of cardiolipin was increased 1.75-fold in the MIDAS-expressing transfectant and decreased 0.65-fold in the downregulated transfectant, when normalized to that of phosphatidylcholine. Thus, the amount of cardiolipin varied more than 2.6-fold with the up- and downregulation of MIDAS.

Mitochondrial DNA, RNA and proteins were not affected by MIDAS

To understand the mitochondrial increase induced by MIDAS, we examined other mitochondrial components, mitochondrial DNA, RNA and proteins (Fig. 7C). The amount of mtDNA was analyzed by Southern blotting and no significant change was observed. Northern blotting also revealed no change in the stationary amounts of COX II mRNA transcribed from mtDNA. Immunoblots revealed no increase in mitochondrion-

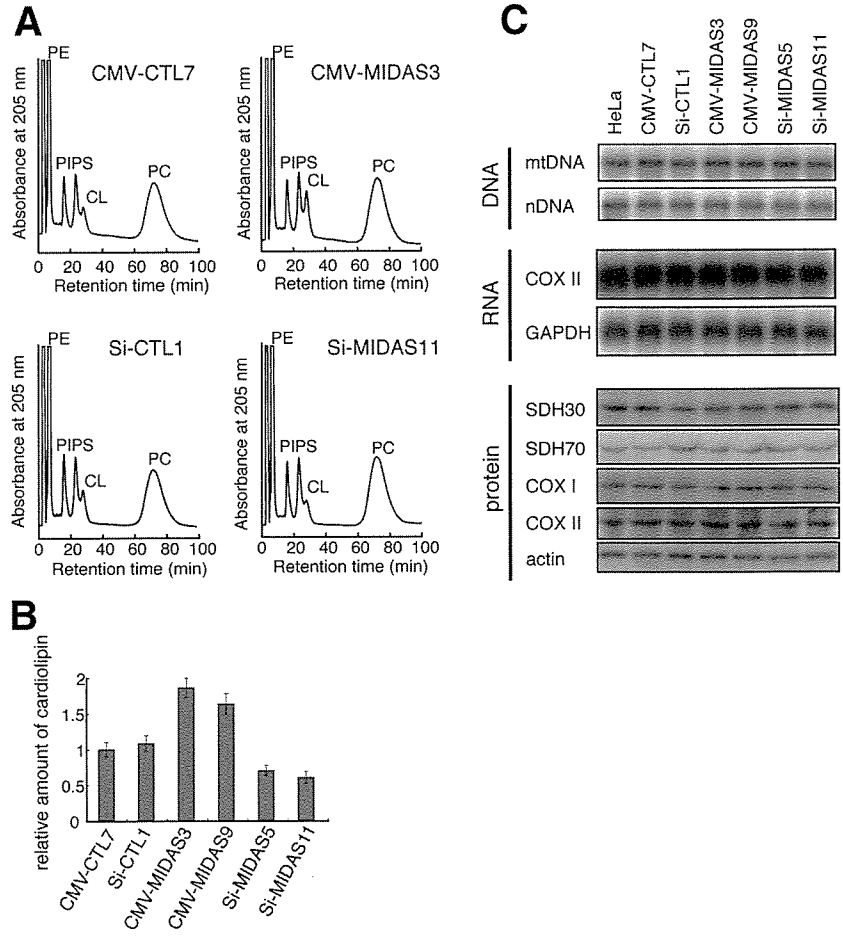

Fig. 7. Effects of MIDAS on amounts of cardiolipin (a mitochondria-specific lipid), mitochondrial DNA, RNA and proteins. (A) Total lipids were extracted from control transfectants (CMV-CTL7 and Si-CTL1), *MIDAS* transfectants (CMV-MIDAS3) and siRNA *MIDAS* transfectants (Si-MIDAS11) and fractionated by HPLC as described in the Materials and Methods. The elution of phospholipids was monitored at 205 nm. CL, cardiolipin; PC, phosphatidylcholine; PE, phosphatidylethanolamine; PI, phosphatidylinositol; PS, phosphatidylserine. (B) The amount of cardiolipin in the transfectants was quantified based on the values in A and normalized to that of phosphatidylcholine. Mean values for three sets of experiments are shown with the s.d. (C) The amount of DNA in HeLa cells and transfectants was analyzed by Southern blotting. To detect mtDNA we used the COX II region in mtDNA as a probe. The nDNA (nuclear DNA) was a loading control and the 18S ribosomal DNA region was used as a probe. The expression of mtDNA and nDNA was analyzed by northern blotting. Blots of total RNA extracted from HeLa and transfectants were hybridized with *COX II*- and *GAPDH* -specific probes. Proteins were analyzed by western blotting. SDH30 and SDH70 are the nucleus-encoded 30 kDa and 70 kDa subunit of SDH, respectively. COX I and COX II are the mitochondrial DNA-encoded subunits.

encoded proteins, COX I and COX II and nucleus-encoded mitochondrial proteins, the 30 kDa and 70 kDa subunits of SDH.

Discussion

In this study, we found three nuclear genes that respond to the depletion of mtDNA. Although mtDNA was completely depleted after a long exposure of HeLa cells to ethidium bromide, its nuclear genes may be affected at a high frequency. Thus, we used a cybrid clone, Ft2-11, that had been obtained by the intercellular transfer of wild-type mitochondria into EB8 cells as a control instead of parental HeLa cells. This procedure, cell fusion between enucleated cells (mitochondrion donor) and EB8 cells, would cause no damage to the nuclear genes.

On comparing the mRNA isolated from EB8 cells with that of control cells by differential display, we found three genes whose expression was higher in EB8 cells. Two of them were the apurinic/apyrimidinic endonuclease I (APE1/HAP1) (Demple et al., 1991) and DNA ligase III genes (Wei et al., 1995). These gene products are located in mitochondria as well as the nucleus and are involved in DNA repair. Thus, it is reasonable to assume that the mitochondrial repair system responds to the depletion of mtDNA.

The third gene product, named MIDAS here, was identical to a Golgi protein, GPP34. The nucleotide sequence of *MIDAS/GPP34* is conserved from yeast to human (Bell et al., 2001; Wu et al., 2000). Its yeast *Saccharomyces cerevisiae* homolog (YDR372c) has been deleted revealing that the gene is not essential for viability (Winzeler et al., 1999; Bidlingmaier and Snyder, 2002). Although a mutation in the YDR372c gene revealed a phenotype with an abnormal budding (Bidlingmaier and Snyder, 2002) and aberrant in protein-vacuolar targeting (Bonangelino et al., 2002), the molecular function of the gene product remains unknown. Genetic analysis showed that there are genetic interactions between YDR372c and intracellular protein-transport factors (RIC1 and YPT6) (Tong et al., 2004). As MIDAS has a leucine-zipper motif (supplementary material Fig. S1), it may interact with a protein involved in intracellular protein transport through this motif.

In most mitochondrial diseases, mutant mtDNA coexists with wild-type mtDNA at various ratios in a heteroplasmic manner and exhibits a cognate pathological phenotype in a threshold-dependent manner. COX-deficient cells have abundant mutant mtDNA, whereas COX-positive cells have a small amount of mutant mtDNA. MIDAS was shown to be more abundant in muscle cells with no COX activity in patients with mitochondrial diseases. This finding indicates that the enhanced expression of MIDAS occurs not only in HeLa cells lacking mtDNA, but also in muscle cells with pathogenic mutant mtDNAs, regardless of point mutations or deletions of mtDNA. MIDAS has putative ATF-1 binding sites and the upregulated expression by EWS/ATF-1 chimeric transcription factor was revealed (Jishage et al., 2003). When mitochondrial dysfunction occurs, the expression of MIDAS may be activated by CREB/ATF-1 family transcription factors.

A previous report (Bell et al., 2001) indicated that GPP34 colocalizes only with Golgi, but not mitochondria. When we used the method they described (Bell et al., 2001) with permeabilization pretreatment after fixation, anti-MIDAS antibody stained only the Golgi apparatus (Fig. 3D,E). On the other hand, immunostaining clearly showed that MIDAS colocalized with both mitochondria and the Golgi apparatus when the cells were subjected to the acetate/ethanol pretreatment to permeabilize the mitochondrial membranes. An outer membrane protein (Tom 20) did not require the permeabilization procedure for staining, but the acetate/ethanol procedure was essential for the proteins located inside mitochondria such as cytochrome c, Hsp60 and SDH70 (Fig. 3C and supplementary material Fig. S3). Thus, the discrepancy is fully explained by the difference in the permeabilization method used (Fig. 3). The present result is consistent with the result of a sub-organellar fractionation experiment that showed that MIDAS is present in the intermembrane space. Thus, it is concluded that the antibody against MIDAS/GPP34 cannot access the mitochondrial MIDAS without the permeabilization pretreatment. As MIDAS lacks typical sequences that could target mitochondria or the Golgi apparatus, it is unknown how it is directed to the respective organelle.

As MIDAS/GPP34 has an isoform, named GPP34R, one may target mitochondria and the other may target the Golgi apparatus. However, this is unlikely because GPP34R was expressed at a level less than 2% of that of MIDAS in HeLa cells. This small amount cannot account for the relative amount of the protein located in the Golgi apparatus. In addition, we performed a crucial experiment. As the fusion protein comprising Myc-tag and the N-terminus of MIDAS targets only Golgi, the N-terminal region may be responsible for targeting mitochondria. In contrast, an alternative fusion protein with Myc-tag at the C-terminus of MIDAS targets mitochondria. This experiment suggests that the single molecule has the potential to localize to two distinct organelles. Further experiments will reveal which location of MIDAS contributes to its distribution.

Mitochondria gathered around the nucleus in MIDAS-expressing transfectants. As mitochondria often gather around the nucleus in sick cells regardless of internal or external conditions, it may be that toxicity of MIDAS forces mitochondria to concentrate around the nucleus by affecting the cytoskeletal structure. However, no abnormal cytoskeletal structure was found in MIDAS-expressing transfectants (supplementary material Fig. S6). Thus, the mitochondrial accumulation was not due to abnormality of the cytoskeleton. The mitochondrial biogenesis occurs near the nucleus and fresh mitochondria are transported to peripheral areas (Yaffe, 1999). Thus, newly synthesized mitochondria seem to be concentrated around the nucleus and then the excess mitochondria may push up the nucleus as seen in Fig. 5B and Fig. 6D, second panel.

A transcriptional coactivator PGC-1 enhances the expression of many mitochondrial proteins by activating several transcription factors, such as NRF-1, NRF-2, Sp1, YY1, CREB and MEF-2/E-box (Scarpulla, 2002). Recognition sites for NRF-1, NRF-2 and Sp1 are common to most nuclear genes encoding components involved in mitochondrial respiration, transcription and replication (Scarpulla, 2002). However, it is unknown how PGC-1 contributes to the increase in mitochondrial lipids. In addition, there has been no report that PGC-1 is expressed in response to mitochondrial dysfunction or damage. MIDAS seems to accumulate mitochondria by an

alternative pathway from PGC-1 because MIDAS did not enhance mitochondrial transcription (Fig. 7C).

As mitochondria dynamically repeat fusion and fission, it is difficult to clarify their number (Griparic and van der Bliek, 2001; Westermann, 2002). In this study, we thus paid attention to the total mass of mitochondria. Three-dimensional imaging revealed a change in the total mass of mitochondria. The increase was 1.6-fold, which agrees with the increase in strength of the fluorescence of MitoTracker Red and MitoTracker Green in MIDAS-expressing transfectants. This increase is not so small because mitochondria occupy more than 20% of the total volume of the cytoplasm in HeLa cells. When the downregulation and upregulation of MIDAS were compared, the total mass was found to vary more than 2.3-fold from 15% to 35% of the total cytoplasm of HeLa cells. Thus, MIDAS dramatically regulates the total mitochondrial mass.

Mitochondria are often swollen pathogenically or by an increase of cytosolic Ca^{2+}. It may be that the mitochondria are simply swollen owing to the expression of MIDAS. However, this is unlikely for the following reasons. First, the ratio of the intensity in red to the intensity in green was the same in all the cells examined, indicating that MIDAS does not exert any influence on membrane potential (Fig. 6C). Although MIDAS-expressing cells have lower concentrations of mitochondrial protein per volume than controls (Fig. 7C), the levels seem high enough for membrane potential. Second, the downregulation of MIDAS conversely decreased the total mass of mitochondria. Third, mitochondria appear intact morphologically, being independent of the up- or downregulation of MIDAS (Fig. 5C). Finally, it is crucial that the amount of cardiolipin varied depending upon the amount of MIDAS and that the extent of the change was well correlated with the total mass of mitochondria that was revealed by three-dimensional imaging. Cardiolipin is a mitochondrion-specific lipid but accounts for only 20% of mitochondrial lipids. This suggests that not only the amount of cardiolipin but also the total amount of mitochondrial lipids is changed by MIDAS. Taken together, it is concluded that total mitochondrial mass is regulated by MIDAS through the biogenesis of mitochondrial lipids.

The molecular mechanism by which the MIDAS protein increases production of cardiolipin is unknown. A detailed analysis of the *MIDAS* gene and the function of MIDAS should provide insight into the molecular mechanism by which mitochondrial dysfunction is sensed to increase mitochondria. The fact that MIDAS is colocalized with both mitochondria and the Golgi apparatus may be a key to answering the question of how lipids contribute to mitochondrial accumulation.

We thank K. Mihara of Kyushu University for the gift of anti-Tom20 and anti-Tom40 antibodies, I. Ohsawa and T. Kanamori for helpful advice and K. Yamagata for technical assistance.

References

Amuthan, G., Biswas, G., Zhang, S. Y., Klein-Szanto, A., Vijayasarathy, C. and Avadhani, N. G. (2001). Mitochondria-to-nucleus stress signaling induces phenotypic changes, tumor progression and cell invasion. *EMBO J.* **20**, 1910-1920.

Asoh, S., Mori, T., Hayashi, J. and Ohta, S. (1996). Expression of the apoptosis-mediator Fas is enhanced by dysfunctional mitochondria. *J. Biochem. (Tokyo)* **120**, 600-607.

Attardi, G. and Schatz, G. (1988). Biogenesis of mitochondria. *Annu. Rev. Cell Biol.* **4**, 289-333.

Bell, A. W., Ward, M. A., Blackstock, W. P., Freeman, H. N., Choudhary, J. S., Lewis, A. P., Chotai, D., Fazel, A., Gushue, J. N., Paiement, J. et al. (2001). Proteomics characterization of abundant Golgi membrane proteins. *J. Biol. Chem.* **276**, 5152-5165.

Bereiter-Hahn, J. and Voth, M. (1994). Dynamics of mitochondria in living cells: shape changes, dislocations, fusion and fission of mitochondria. *Microsc. Res. Tech.* **27**, 198-219.

Bidlingmaier, S. and Snyder, M. (2002). Large-scale identification of genes important for apical growth in *Saccharomyces cerevisiae* by directed allele replacement technology (DART) screening. *Funct. Integr. Genomics* **1**, 345-356.

Biswas, G., Adebanjo, O. A., Freedman, B. D., Anandatheerthavarada, H. K., Vijayasarathy, C., Zaidi, M., Kotlikoff, M. and Avadhani, N. G. (1999). Retrograde Ca^{2+} signaling in C2C12 skeletal myocytes in response to mitochondrial genetic and metabolic stress: a novel mode of inter-organelle crosstalk. *EMBO J.* **18**, 522-533.

Bonangelino, C. J., Chavez, E. M. and Bonifacino, J. S. (2002). Genomic screen for vacuolar protein sorting genes in *Saccharomyces cerevisiae*. *Mol. Biol. Cell* **13**, 2486-2501.

Brunk, C. F. (1981). Mitochondrial proliferation during myogenesis. *Exp. Cell Res.* **136**, 305-309.

Collins, T. J., Berridge, M. J., Lipp, P. and Bootman, M. D. (2002). Mitochondria are morphologically and functionally heterogeneous within cells. *EMBO J.* **21**, 1616-1627.

Cortopassi, G. A. and Wong, A. (1999). Mitochondria in organismal aging and degeneration. *Biochim. Biophys. Acta* **1410**, 183-193.

Demple, B., Herman, T. and Chen, D. S. (1991). Cloning and expression of APE, the cDNA encoding the major human apurinic endonuclease: definition of a family of DNA repair enzymes. *Proc. Natl. Acad. Sci. USA* **88**, 11450-11454.

Dubowitz, V. (1985). Histological and histochemical stains and reactions. In *Muscle Biopsy: a practical approach*, 2nd edn, (ed. V. Dubowitz), pp. 19-40. London: Balliere Tindall.

Engel, W. K. and Cunningham, G. G. (1963). Rapid examination of muscle tissue. An improved trichrome method for fresh-frozen biopsy sections. *Neurology* **13**, 919-926.

Erlich, R., Gleeson, P. A., Campbell, P., Dietzsch, E. and Toh, B. H. (1996). Molecular characterization of *trans*-Golgi p230. A human peripheral membrane protein encoded by a gene on chromosome 6p12-22 contains extensive coiled-coil alpha-helical domains and a granin motif. *J. Biol. Chem.* **271**, 8328-8337.

Folch, J., Lees, M. and Sloane Stanley, G. H. (1957). A simple method for the isolation and purification of total lipides from animal tissues. *J. Biol. Chem.* **226**, 497-509.

Garesse, R. and Vallejo, C. G. (2001). Animal mitochondrial biogenesis and function: a regulatory cross-talk between two genomes. *Gene* **263**, 1-16.

Goglia, F., Moreno, M. and Lanni, A. (1999). Action of thyroid hormones at the cellular level: the mitochondrial target. *FEBS Lett.* **452**, 115-120.

Goto, Y., Nonaka, I. and Horai, S. (1990). A mutation in the $tRNA^{Leu(UUR)}$ gene associated with the MELAS subgroup of mitochondrial encephalomyopathies. *Nature* **348**, 651-653.

Green, D. R. and Kroemer, G. (2004). The pathophysiology of mitochondrial cell death. *Science* **305**, 626-629.

Griparic, L. and van der Bliek, A. M. (2001). The many shapes of mitochondrial membranes. *Traffic* **2**, 235-244.

Hansson, A., Hance, N., Dufour, E., Rantanen, A., Hultenby, K., Clayton, D. A., Wibom, R. and Larsson, N. G. (2004). A switch in metabolism precedes increased mitochondrial biogenesis in respiratory chain-deficient mouse hearts. *Proc. Natl. Acad. Sci. USA* **101**, 3136-3141.

Hasegawa, H., Matsuoka, T., Goto, Y. and Nonaka, I. (1991). Strongly succinate dehydrogenase-reactive blood vessels in muscles from patients with mitochondrial myopathy, encephalopathy, lactic acidosis and stroke-like episodes. *Ann. Neurol.* **29**, 601-605.

Hayashi, J., Ohta, S., Kikuchi, A., Takemitsu, M., Goto, Y. and Nonaka, I. (1991). Introduction of disease-related mitochondrial DNA deletions into HeLa cells lacking mitochondrial DNA results in mitochondrial dysfunction. *Proc. Natl. Acad. Sci. USA* **88**, 10614-10618.

Hayashi, J., Ohta, S., Kagawa, Y., Kondo, H., Kaneda, H., Yonekawa, H., Takai, D. and Miyabayashi, S. (1994). Nuclear but not mitochondrial genome involvement in human age-related mitochondrial dysfunction. Functional integrity of mitochondrial DNA from aged subjects. *J. Biol. Chem.* **269**, 6878-6883.

Holt, I. J., Harding, A. E. and Morgan-Hughes, J. A. (1988). Deletions of muscle mitochondrial DNA in patients with mitochondrial myopathies. *Nature* **331**, 717-719.

Jishage, M., Fujino, T., Yamazaki, Y., Kuroda, H. and Nakamura, T. (2003). Identification of target genes for EWS/ATF-1 chimeric transcription factor. *Oncogene* **22**, 41-49.

Kanamori, T., Nishimaki, K., Asoh, S., Ishibashi, Y., Takata, I., Kuwabara, T., Taira, K., Yamaguchi, H., Sugihara, S., Yamazaki, T. et al. (2003). Truncated product of the bifunctional *DLST* gene involved in biogenesis of the respiratory chain. *EMBO J.* **22**, 2913-2923.

Kang, D. and Hamasaki, N. (2002). Maintenance of mitochondrial DNA integrity: repair and degradation. *Curr. Genet.* **41**, 311-322.

Kawahara, H., Houdou, S. and Inoue, T. (1991). Scanning electron microscopic observations on muscle cells of experimental mitochondrial myopathy produced by 2, 4-dinitrophenol. *J. Submicrosc. Cytol. Pathol.* **23**, 397-403.

Klaus, S., Casteilla, L., Bouillaud, F. and Ricquier, D. (1991). The uncoupling protein UCP: a membraneous mitochondrial ion carrier exclusively expressed in brown adipose tissue. *Int. J. Biochem.* **23**, 791-801.

Kobayashi, Y., Momoi, M. Y., Tominaga, K., Momoi, T., Nihei, K., Yanagisawa, M., Kagawa, Y. and Ohta, S. (1990). A point mutation in the mitochondrial $tRNA^{Leu(UUR)}$ gene in MELAS (mitochondrial myopathy, encephalopathy, lactic acidosis and stroke-like episodes). *Biochem. Biophys. Res. Commun.* **173**, 816-822.

Kobayashi, Y., Momoi, M. Y., Tominaga, K., Shimoizumi, H., Nihei, K., Yanagisawa, M., Kagawa, Y. and Ohta, S. (1991). Respiration-deficient cells are caused by a single point mutation in the mitochondrial $tRNA^{Leu(UUR)}$ gene in mitochondrial myopathy, encephalopathy, lactic acidosis and strokelike episodes (MELAS). *Am. J. Hum. Genet.* **49**, 590-599.

Kowaltowski, A. J. and Vercesi, A. E. (1999). Mitochondrial damage induced by conditions of oxidative stress. *Free Radic. Biol. Med.* **26**, 463-471.

Kroemer, G. and Reed, J. C. (2000). Mitochondrial control of cell death. *Nat. Med.* **6**, 513-519.

Liang, P. and Pardee, A. B. (1992). Differential display of eukaryotic messenger RNA by means of the polymerase chain reaction. *Science* **257**, 967-971.

Lightowlers, R. N., Chinnery, P. F., Turnbull, D. M. and Howell, N. (1997). Mammalian mitochondrial genetics: heredity, heteroplasmy and disease. *Trends Genet.* **13**, 450-455.

Melov, S. (2000). Mitochondrial oxidative stress. Physiologic consequences and potential for a role in aging. *Ann. New York Acad. Sci.* **908**, 219-225.

Moraes, C. T., Ricci, E., Bonilla, E., DiMauro, S. and Schon, E. A. (1992). The mitochondrial $tRNA^{Leu(UUR)}$ mutation in mitochondrial encephalomyopathy, lactic acidosis and strokelike episodes (MELAS): genetic, biochemical and morphological correlations in skeletal muscle. *Am. J. Hum. Genet.* **50**, 934-949.

Moyes, C. D., Mathieu-Costello, O. A., Tsuchiya, N., Filburn, C. and Hansford, R. G. (1997). Mitochondrial biogenesis during cellular differentiation. *Am. J. Physiol.* **272**, C1345-C1351.

Muller-Hocker, J., Pongratz, D. and Hubner, G. (1986). Activation of mitochondrial ATPase as evidence of loosely coupled oxidative phosphorylation in various skeletal muscle disorders. A histochemical fine-structural study. *J. Neurol. Sci.* **74**, 199-213.

Munro, S. and Pelham, H. R. (1987). A C-terminal signal prevents secretion of luminal ER proteins. *Cell* **48**, 899-907.

Nisoli, E., Clementi, E., Paolucci, C., Cozzi, V., Tonello, C., Sciorati, C., Bracale, R., Valerio, A., Francolini, M., Moncada, S. et al. (2003). Mitochondrial biogenesis in mammals: the role of endogenous nitric oxide. *Science* **299**, 896-899.

Nisoli, E., Falcone, S., Tonello, C., Cozzi, V., Palomba, L., Fiorani, M., Pisconti, A., Brunelli, S., Cardile, A., Francolini, M. et al. (2004). Mitochondrial biogenesis by NO yields functionally active mitochondria in mammals. *Proc. Natl. Acad. Sci. USA* **101**, 16507-16512.

Ohta, S. (2003). A multi-functional organelle mitochondrion is involved in cell death, proliferation and disease. *Curr. Med. Chem.* **10**, 2485-2494.

Pfanner, N. and Geissler, A. (2001). Versatility of the mitochondrial protein import machinery. *Nat. Rev. Mol. Cell. Biol.* **2**, 339-349.

Scarpulla, R. C. (2002). Nuclear activators and coactivators in mammalian mitochondrial biogenesis. *Biochim. Biophys. Acta* **1576**, 1-14.

Schon, E. A. (2000). Mitochondrial genetics and disease. *Trends Biochem. Sci.* **25**, 555-560.

Shoubridge, E. A., Karpati, G. and Hastings, K. E. (1990). Deletion mutants are functionally dominant over wild-type mitochondrial genomes in skeletal muscle fiber segments in mitochondrial disease. *Cell* **62**, 43-49.

Tong, A. H., Lesage, G., Bader, G. D., Ding, H., Xu, H., Xin, X., Young, J., Berriz, G. F., Brost, R. L., Chang, M. et al. (2004). Global mapping of the yeast genetic interaction network. *Science* **303**, 808-813.

Trounce, I. A., Kim, Y. L., Jun, A. S. and Wallace, D. E. (1996). Assessment of mitochondrial oxidative phosphorylation in patient muscle biopsies, lymphoblasts and transmitochondrial cell lines. *Methods Enzymol.* **264**, 484-509.

Vorobjev, I. A. and Zorov, D. B. (1983). Diazepam inhibits cell respiration and induces fragmentation of mitochondrial reticulum. *FEBS Lett.* **163**, 311-314.

Wallace, D. C. (1999). Mitochondrial diseases in man and mouse. *Science* **283**, 1482-1488.

Weber, K., Ridderskamp, D., Alfert, M., Hoyer, S. and Wiesner, R. J. (2002). Cultivation in glucose-deprived medium stimulates mitochondrial biogenesis and oxidative metabolism in HepG2 hepatoma cells. *Biol. Chem.* **383**, 283-290.

Wei, Y. F., Robins, P., Carter, K., Caldecott, K., Pappin, D. J., Yu, G. L., Wang, R. P., Shell, B. K., Nash, R. A., Schar, P. et al. (1995). Molecular cloning and expression of human cDNAs encoding a novel DNA ligase IV and DNA ligase III, an enzyme active in DNA repair and recombination. *Mol. Cell. Biol.* **15**, 3206-3216.

Westermann, B. (2002). Merging mitochondria matters: Cellular role and molecular machinery of mitochondrial fusion. *EMBO Rep.* **3**, 527-531.

Winzeler, E. A., Shoemaker, D. D., Astromoff, A., Liang, H., Anderson, K., Andre, B., Bangham, R., Benito, R., Boeke, J. D., Bussey, H. et al. (1999). Functional characterization of the *S. cerevisiae* genome by gene deletion and parallel analysis. *Science* **285**, 901-906.

Wu, C. C., Taylor, R. S., Lane, D. R., Ladinsky, M. S., Weisz, J. A. and Howell, K. E. (2000). GMx33: a novel family of *trans*-Golgi proteins identified by proteomics. *Traffic* **1**, 963-975.

Yaffe, M. P. (1999). The machinery of mitochondrial inheritance and behavior. *Science* **283**, 1493-1497.

Zeller, R. (1998). Preparation of cells and tissues for fluorescence microscopy. In *Cells: A Laboratory Manual. Volume 3 Subcellular localization of genes and their products.* (ed. D. L. Spector, R. D. Goldman and L. A. Leinwand), pp. 98.01-98.20. New York: Cold Spring Harbor Laboratory Press.

Cell Death and Differentiation (2005) 12, 384–394

www.nature.com/cdd

Zonal necrosis prevented by transduction of the artificial anti-death FNK protein

S Asoh[1], T Mori[2], S Nagai[1], K Yamagata[1], K Nishimaki[1], Y Miyato[1], Y Shidara[1,3] and S Ohta*[,1]

[1] Department of Biochemistry and Cell Biology, Institute of Development and Aging Sciences, Graduate School of Medicine, Nippon Medical School, Kawasaki-city, Kanagawa, Japan
[2] Saitama Medical Center/School, Kawagoe, Saitama, Japan
[3] Department of Pathology, Tokyo Women's Medical University, School of Medicine, Shinjuku-ku, Tokyo, Japan
* Corresponding author: S Ohta, Department of Biochemistry and Cell Biology, Institute of Development and Aging Sciences, Graduate School of Medicine, Nippon Medical School, Kawasaki-city, Kanagawa 211-8533, Japan. Tel: +81 44 733 9267; Fax: +81 44 733 9268; E-mail: ohta@nms.ac.jp

Received 28.6.04; revised 15.11.04; accepted 26.11.04; published online 04.2.05
Edited by H Ichijo

Abstract

Protection of cells from necrosis would be important for many medical applications. Here, we show protein transduction domain (PTD)-FNK therapeutics based on protein transduction to prevent necrosis and acute hepatic injury with zonal death induced by carbon tetrachloride (CCl_4). PTD-FNK is a fusion protein comprising the HIV/Tat PTD and FNK, a gain-of-function mutant of anti-apoptotic Bcl-x_L. PTD-FNK protected hepatoma HepG2 from necrotic death induced by CCl_4, and additionally, increased the apoptotic population among cells treated with CCl_4. A concomitant treatment with a pan-caspase inhibitor Z-VAD-FMK (N-benzyloxycarbonyl-Val-Ala-Asp-fluoromethylketone), which alone could not prevent the necrosis, protected these cells from the apoptosis. When pre-injected intraperitoneally, PTD-FNK markedly reduced zonal liver necrosis caused by CCl_4. Moreover, injection of PTD-FNK accompanied by Z-VAD-FMK suppressed necrotic injury even after CCl_4 administration. These results suggest that PTD-FNK has great potential for clinical applications to prevent cell death, whether from apoptosis or necrosis, and organ failure.

Cell Death and Differentiation (2005) **12**, 384–394.
doi:10.1038/sj.cdd.4401569
Published online 4 February 2005

Keywords: necrosis; apoptosis; protein transduction domain; carbon tetrachloride; HepG2; liver; Bcl-x_L; protein therapeutics

Abbreviations: Ac-DEVD-AMC, *N*-acetyl-Asp-Glu-Val-Asp-7-amino-4-methylcoumarin; Ac-DEVD-CHO, *N*-acetyl-Asp-Glu-Val-Asp-CHO (aldehyde); ALT, alanine amino transferase; AST, aspartate amino transferase; CCl_4, carbon tetrachloride; DMEM, Dulbecco's modified Eagle's medium; ER, endoplasmic reticulum; *i.p.*, intraperitoneally; *s.c.*, subcutaneously; DEX, dexamethasone; TNFα, tumor necrosis factor α; CHX, cycloheximide; PARP-1, poly(ADP-ribose) polymerase; PI, propidium iodide; PTD, protein transduction domain; STS, staurosporine; Z-VAD-FMK, *N*-benzyloxycarbonyl-Val-Ala-Asp-fluoromethylketone; TUNEL, terminal deoxynucleotidyl transferase-mediated dUTP nick-end labeling

Introduction

Necrosis is morphologically distinct from apoptosis and defined as cell death accompanied by a rapid efflux of cell constituents to the extracellular space due to a loss of cytoplasmic membrane integrity.[1] Necrosis usually takes place under extremely harmful environmental conditions such as exposure to toxic chemicals, physical insults, and microbial pathogens and causes inflammation, which in turn gives rise to serious damage to surrounding cells.[2] Inflammatory responses can be controlled with anti-inflammatory agents, but necrosis itself cannot.[3–5] Therefore, it is very important to reduce or prevent necrosis as a primary cause.

Anti-apoptotic proteins would provide novel means for therapeutic intervention to prevent massive cell death accompanying cell toxic injuries. In fact, a great number of studies have shown that anti-apoptotic members of the Bcl-2 family, Bcl-2 and Bcl-x_L, inhibit apoptosis of cultured cells induced by various death stimuli.[6–11] On the other hand, a few *in vitro* studies[12,13] showed that the proteins prevent necrotic cell death caused by a limited kind of death stimulus such as hyposia, where necrosis coexists with apoptosis. In these cases, necrosis appeared to be initiated by apoptosis-inducing reagents, and then ATP depletion resulted in a necrotic morphology. Thus, the anti-apoptotic proteins seem to exhibit anti-cell death activity against some forms of necrosis, which involve apoptotic machinery to some extent.

FNK (originally designated Bcl-xFNK in Asoh *et al.*[14]) was constructed from Bcl-x_L by the site-directed mutagenesis of three amino acids (Y22*F*/ Q26*N*/ R165*K*) to strengthen cytoprotective activity. FNK is the sole mutant with a gain-of-function phenotype among the mammalian anti-apoptotic factors, as FNK exhibited the stronger anti-apoptotic activity than Bcl-x_L to protect cultured cells from death induced by various death stimuli including oxidative stress, a calcium ionophore (A23187) and withdrawal of growth factors.[14] It has been shown that proteins are directly and readily introduced into cells regardless of their molecular size when fused with the PTD (protein transduction domain) of HIV/Tat protein.[15] PTD-fused proteins can be delivered to several tissues, including the brain, when injected into mice systemically.[16] In addition, PTD-FNK, a fusion protein of the PTD and FNK, penetrates the dense matrix of cartilage to reach chondrocytes.[17] In a previous study, PTD-FNK was demonstrated to reduce ischemic injury to hippocampal CA1 neurons after a transient forebrain ischemia,[18] which involves slow progressive neuronal degeneration, and an apoptotic pathway is suggested to contribute to the ischemic degeneration, to some extent.[19]

The enhanced cytoprotective activity of FNK against oxidative stress and a calcium ionophore give rise to the possibility that FNK effectively protects cells from necrosis as well as apoptosis, because oxidative stress[20–22] and a disruption of calcium homeostasis[23–25] are known to induce necrosis. Carbon tetrachloride (CCl_4) has been used to induce necrosis in control experiments for studies on apoptosis[26–29] and is one of most typical model agents for studying the pathogenesis of liver injury. The hepatotoxicity of CCl_4 *in vivo* has been well studied, indicating the importance of the reductive dehalogenation of CCl_4 catalyzed by cytochrome P450 in the endoplasmic reticulum (ER) as the initial event of the toxic cascades,[30–34] and it is widely accepted that CCl_4 causes hepatic centrilobular necrosis.

Here, we show that the treatment of mice with PTD-FNK mitigated liver injury, including zonal necrosis, induced by CCl_4.

Results

Necrosis in HepG2 induced by CCl_4

We used a cell line HepG2 derived from hepatocyte cells as in *in vitro* experiments. HepG2 started to die in Dulbecco's modified Eagle's medium (DMEM) containing 80% saturation of CCl_4 in the absence of serum at 4 h and the survival rate at 8 h was 5.5% (Figure 1a). Thus, the CCl_4-induced death is not due to an immediate damage by CCl_4 as reported.[35] Nuclear staining with propidium iodide (PI)/Hoechst 33342 showed that PI-positive cells increased in number with time and that a majority of dead cells had a round nucleus uniformly stained with PI (Figure 1e). Their nuclear morphology is different from that of the cells killed by staurosporine (STS), which clearly caused nuclear fragmentation, one of the typical features of apoptosis (Figure 2c, top left panel). To characterize biochemically the death form of HepG2 cells treated with CCl_4, caspase-3/caspase-3-like activity, DNA fragmentation (laddering) and cleavage pattern of poly(ADP-ribose) polymerase-1 (PARP-1) were compared among the cells treated with CCl_4, STS and tumor necrosis factor α (TNFα). STS induced caspase-3-like activity at 4 h, with a plateau reached at 6 h, but CCl_4 had no effect even at 8 h (Figure 1b). DNA fragmentation was detected at 6 h and clearly observed at 8 h in STS-treated, but not CCl_4-treated cells (Figure 1c). TNFα with cycloheximide (CHX) is known to induce apoptosis in HepG2.[36,37] PARP-1, a target of caspase-3, was cleaved into apoptotic fragments including the 85 kDa polypeptide in cells treated with TNFα/CHX (Figure 1d, indicated by an asterisk). In contrast, a fragment of 50 kDa, derived from PARP-1, clearly appeared in the CCl_4-treated cells at 4 h and decreased at 8 h (Figure 1d, indicated by an arrow). The 50 kDa fragment was designated as a major necrotic fragment.[38–40] From these results, we confirmed that the death of HepG2 cells induced by CCl_4 is predominantly due to necrosis.

Protection of HepG2 from TNFα/CHX-induced apoptotic death by FNK transduction

PTD-FNK was shown to readily enter cultured cells of a neuroblastoma, SH-SY5Y, in 30 min to 1 h in a previous study.[18] A pleiotropic cytokine, TNFα, has been shown to induce apoptosis and be involved in acute CCl_4-induced hepatic injury.[41–43] We investigated whether PTD-FNK prevents HepG2 from TNFα/CHX-induced apoptosis. Cells were pretreated with PTD-FNK and incubated with TNFα/CHX in the presence of PTD-FNK. PTD-FNK significantly protected HepG2 against the cytotoxicity of TNFα (Figure 2).

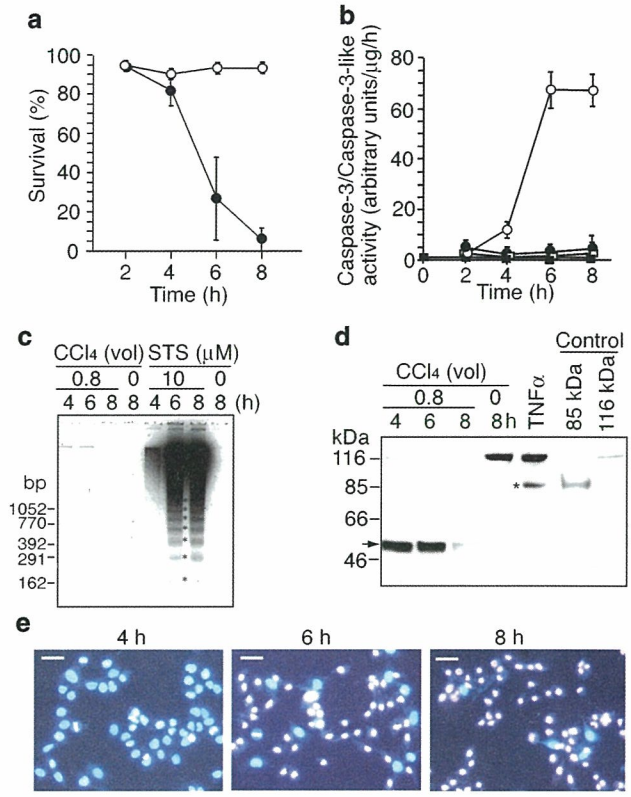

Figure 1 CCl_4 induces necrotic death of HepG2. (**a**) Cells were incubated with DMEM lacking FBS in the presence (closed circle) or absence (open circle) of 80%-saturated CCl_4 for the indicated time periods. The cells were stained with Hoechst 33342 and PI to calculate survival (%); 100 × Hoechst-stained cells/(Hoechst-stained cells + PI-stained cells). The mean of four independent wells (four fields of view per well) is shown with the S.D. (vertical bars). (**b**) Cells were incubated with the complete medium in the presence (open circle) or absence (closed circle) of STS, or with DMEM lacking FBS in the presence (open square) or absence (closed square) of 80%-saturated CCl_4 for the indicated time periods. The cells were harvested to prepare cell lysates for the caspase-3/caspase-3-like activity assay. The enzyme activity (mean with S.D.) is shown as arbitrary units/mg protein/h. (**c**) Cells were treated with CCl_4 or STS as described in (**b**). The harvested cells were treated with Triton X-100, and then centrifuged to remove intact nuclei. After propanol precipitation, fragmented DNAs were subjected to agarose gel electrophoresis. The STS-treated cells (8 h) showed a clear DNA ladder (marked with stars). (**d**) Western blot analysis of PARP. Total proteins were prepared from cells treated with CCl_4 for 4, 6 and 8 h, cells treated with DMEM for 8 h and cells treated with TNFα (10 ng/ml) and CHX (10 μg/ml) for 7 h, as described in Materials and methods. The total protein (30 μg) was subjected to Western blot analysis using an anti-body against PARP. Jurkat control lysate (BD Biosciences Pharmingen) and HL-60 cell extract (induced by etoposide) (Calbiochem), were also used for controls of the 116 kDa intact and the 85 kDa fragment of human PARP, respectively. The 85 kDa fragment appeared in the cells treated with TNFα (marked with*). An arrow indicates a 50 kDa fragment derived from PARP. (**e**) Representative images of cells incubated with DMEM lacking FBS in the presence of 80%-saturated CCl_4 for the indicated time periods. The cells were stained with Hoechst 33342 and PI. Scale bars: 50 μm

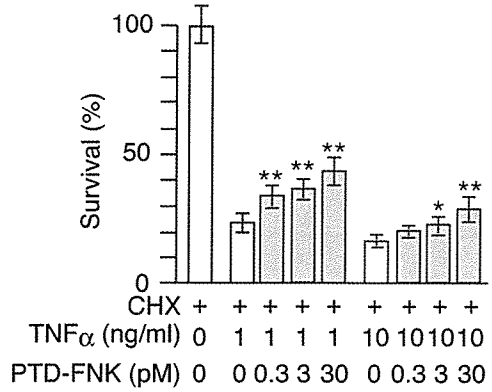

Figure 2 PTD-FNK protects HepG2 against TNFα-induced apoptosis. Cells were washed with FBS-free DMEM, and treated with various concentrations of PTD-FNK in FBS-free DMEM for 1 h, followed by incubation with DMEM containing FBS (10%) and CHX (10 μg/ml) for 30 min. The cells were cultured with TNFα (1 or 10 ng/ml) for 12 h, and cells surviving were enumerated under a microscope by the trypan blue exclusion method. Means of three independent wells are shown with the S.D. Statistical analysis was performed using one-way ANOVA: *, $P<0.05$; **, $P<0.01$, *versus* control

Protection of HepG2 from CCl_4-induced necrotic death by FNK transduction

Next, to examine the cytoprotective effect of PTD-FNK on CCl_4-induced cell death in HepG2, PTD-FNK-pretreated cells were incubated with CCl_4 in the presence of PTD-FNK. Survival rates of the cells treated with PTD-FNK significantly increased up to 3 nM in a concentration-dependent manner and slightly decreased at the higher concentrations (Figure 3a (open bars) and c), indicating that PTD-FNK alone suppresses cell death induced by CCl_4. Comparison of the cytoprotective activity between PTD-FNK and PTD-Bcl-x_L showed that the activity of the former is stronger (Figure 3a and c).

Conversion of necrotic features into apoptotic ones forced by PTD-FNK

During this experiment, we noticed that a substantial population of dying cells treated with PTD-FNK had fragmented nuclei whose morphology was observed when treated with STS (Figure 3c, arrowheads and insets). The population of dead cell carrying a fragmented nucleus increased with the concentration of PTD-FNK, varying from 2.0 to 10% among cells with PTD-FNK treatment (Figure 3a, gray bars).

To confirm whether the dead cells with fragmented nuclei underwent apoptosis, HepG2 cells were exposed to CCl_4 in the presence of Z-VAD-FMK, a cell-permeable pan-caspase inhibitor. Z-VAD-FMK fully inhibited the STS-induced apoptosis of HepG2 (Figure 3c, leftmost panels). Importantly, the survival rate of cells co-treated with PTD-FNK and Z-VAD-FMK was significantly higher than that of cells treated with Z-VAD-FMK alone (Figure 3b). More interestingly, much more of the cells treated with a combination of PTD-FNK or PTD-Bcl-x_L and Z-VAD-FMK were survived than the cells treated with PTD-FNK or PTD-Bcl-x_L alone, and the combination treatment significantly decreased the number of dying cells carrying fragmented nuclei (Figure 3b). These findings strongly suggest that PTD-FNK can protect a majority of HepG2 cells from necrotic death caused by CCl_4, and that PTD-FNK forced the cells in a necrotic pathway into an apoptotic pathway and then Z-VAD-FMK inhibited cell death in the apoptotic pathway.

Furthermore, we tried to detect an early stage of apoptosis by examining the binding of Annexin V to the surface of cells. Cells were exposed to CCl_4 in the absence or presence of PTD-FNK. Some cells were clearly stained with Annexin-V-FLUOS but not with PI (Figure 3e, arrowheads in the lower middle panel). Such Annexin-V-positive and PI-negative cells markedly increased depending upon the addition of PTD-FNK (Figure 3d). In contrast, the Annexin-V-positive and PI-negative population among the cells treated only with CCl_4 was very low and equivalent with that among the cells untreated with CCl_4 (Figure 3d), suggesting that the small population of apoptotic cells was due to the depletion of serum but not by the exposure to CCl_4. Taken together, these results strongly suggest that PTD-FNK leads cells to an apoptotic pathway from the necrotic process induced by CCl_4.

PTD-FNK retains the mitochondrial membrane potential and intracellular ATP level

After entering cells, PTD-FNK localizes to miochondria.[17,18] We examined the levels of intracellular ATP and the mitochondrial membrane potential to reveal the role of PTD-FNK on mitochondrial functions during the protection against necrosis. Exposure against CCl_4 decreased the intracellular ATP and PTD-FNK slightly but significantly suppressed the decrease (Figure 4a). Then, we examined the mitochondria membrane potential in CCl_4-treated cells in the presence or absence of PTD-FNK at 4 h, using mitochondria-specific fluorescent dyes, MitoTracker Red CMXRos and MitoTracker Green FM. MitoTracker Red stains mitochondria, depending upon the membrane potential, while MitoTracker Green FM depends upon the mitochondrial mass in a membrane potential-independent manner. Thus, the relative mitochondrial potential level was estimated by normalizing the red fluorescence with the green one. CCl_4 decreased the membrane potential to 68% of the initial level, and PTD-FNK completely inhibited the decrease (Figure 4b). It is noted that pre-incubation with PTD-FNK did not affect the intracellular ATP levels and the mitochondria membrane potential (Figure 4a and b at 0 time).

Delivery of PTD-FNK into the liver

The tissue delivery of the fused protein, PTD-FNK, injected intraperitoneally (*i.p.*) into 7-week-old male mice was examined by immunohistochemical staining. At 12 h after the injection, exogenous PTD-FNK was detected in the liver by using monoclonal anti-Bcl-x antibody, which recognizes the FNK protein as well as Bcl-x_L (Figure 5a). The protein appeared to be distributed ubiquitously. Next, we tested the delivery of the PTD-FNK protein into liver by injecting subcutaneously (*s.c.*) PTD-FNK. At 1, 3, 5 and 12 h after injection, livers were removed for staining with the monoclonal

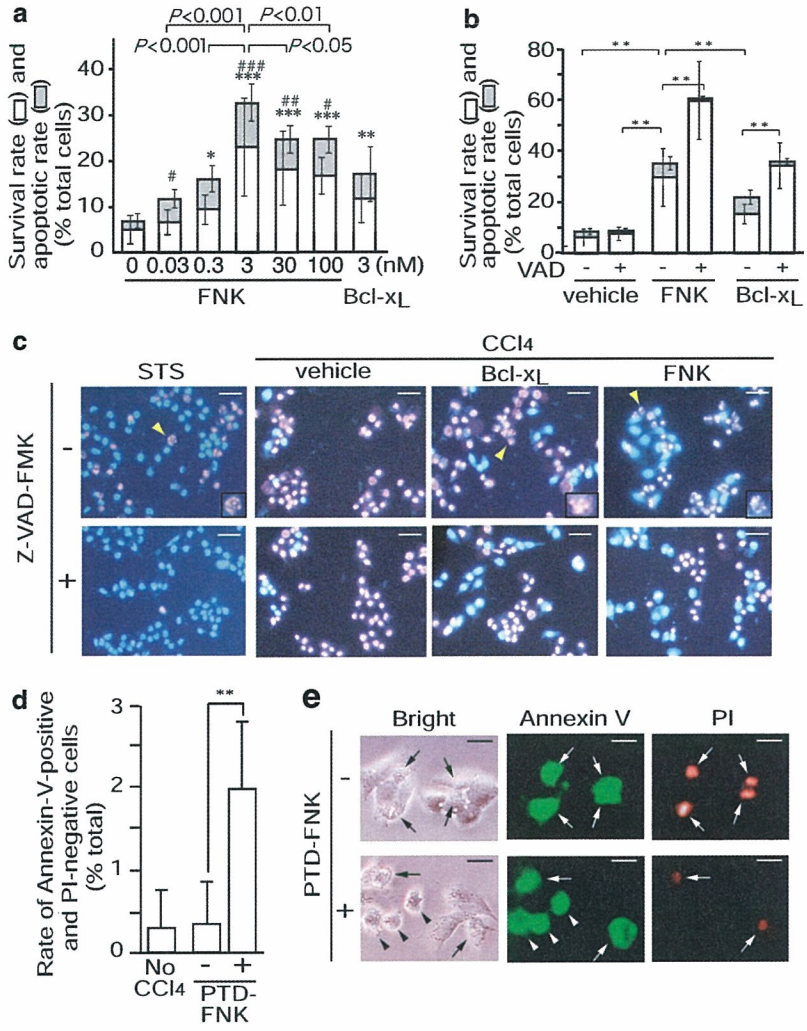

Figure 3 PTD-FNK prevents necrotic death of HepG2. (**a**) Cells were incubated with PTD-FNK (FNK) or PTD-Bcl-x_L (Bcl-x_L) at the indicated concentrations in FBS-free DMEM for 1 h, after washed with FBS-free DMEM. The cells were then treated with 80%-saturated CCl_4 for 8 h in the presence of PTD-FNK (FNK) or PTD-Bcl-x_L (Bcl-x_L) at the indicated concentrations. The cells were stained with Hoechst 33342 and PI to calculate the survival rate (open bar) and apoptotic rate (PI-stained cells with a fragmented nucleus; gray bar) as described in Figure 1a. The mean of four independent wells (four fields of view per well) is shown with the S.D. (vertical bars). Statistical analysis was performed for the suvival rate by one-way ANOVA. *, $P<0.05$; **, $P<0.01$; ***, $P<0.001$, compared with FNK 0 nM.$^{\#}$, $P<0.05$; $^{\#\#}$, $P<0.01$; $^{\#\#\#}$, $P<0.001$, compared with Bcl-xL 3 nM. (**b**) Cells were pre-incubated with vehicle, 3 nM PTD-FNK (FNK) or 3 nM PTD-Bcl-x_L (Bcl-x_L) in FBS-free DMEM in the presence or absence of Z-VAD-FMK (VAD, 50 μM) for 1 h, after washed with FBS-free DMEM. The cells were then treated with 80%-saturated CCl_4 for 8 h in the presence or absence of 3 nM PTD-FNK (FNK), 3 nM PTD-Bcl-x_L (Bcl-x_L) or 50 μM Z-VAD-FMK as indicated. The cells were stained with Hoechst 33342 and PI to calculate the survival rate (open bar) and apoptotic rate (gray bar) as described in Figure 2a. The mean of four independent wells (four fields of view per well) is shown with the S.D.(vertical bars). Statistical analysis was performed for the survival rate using one-way ANOVA: *, $P<0.05$; **, $P<0.001$. (**c**) Representative images of cells described in Figure 2b and cells treated with STS (10 μM) in the presence or absence of Z-VAD-FMK (50 μM) for 12 h. For the cells treated with STS and Z-VAD-FMK, Z-VAD-FMK was added 1 h before the STS treatment. PI-stained cells with a fragmented nucleus are shown by arrowheads and enlarged (insets). Scale bars: 50 μm. (**d**) Cells were pre-incubated with 3 nM PTD-FNK (+) or vehicle (−) in FBS-free DMEM for 1 h, after washed with FBS-free DMEM. The cells pre-treated with PTD-FNK or vehicle were incubated with 80%-saturated CCl_4 containing 3 nM PTD-FNK or vehicle, respectively, for 3 h. Cells without any pre-treatment were also incubated with DMEM lacking FBS (no CCl_4) for 3 h. The cells were stained with Annexin-V-FLUOS and PI to calculate the rate of Annexin-V-positive and PI-negative cells (%); 100 × Annexin-V-positive and PI-negative cells/total cells in a bright field of view. The mean of three independent wells (three to four fields of view per well) is shown with the S.D. (vertical bars). **, $P< 0.0001$ by the Student's *t*-test. (**e**) Representative images of cells described in Figure 2d are shown. Bright, bright field; Annexin V, Annexin-V-FLUOS staining (green); PI, PI staining (red); arrowheads, apoptotic cells; arrows, necrotic or dead cells. Scale bars: 25 μm

anti-Bcl-x antibody. Immunoreactivity was found in the centrilobular region at 1 h and extensive intracellular accumulation of PTD-FNK was observed at 3 h (Figure 5b). The reactivity peaked at 3 h after injection and gradually decreased but clearly remained until 12 h, compared with vehicle injection (Figure 5b and c). Thus, these results indicate that PTD-FNK is promptly delivered to liver by *s.c.* injection as well as *i.p.* administration.

Pre-treatment with PTD-FNK prevents acute liver injury induced by CCl_4

To assess the activity of FNK delivered into the liver to inhibit acute and chronic CCl_4-induced injuries, mice injected with the PTD-FNK protein were treated with CCl_4. Injection of CCl_4 caused a variety of toxic changes such as zonal necrosis, hydropic degeneration of cytoplasm or pyknosis/loss of

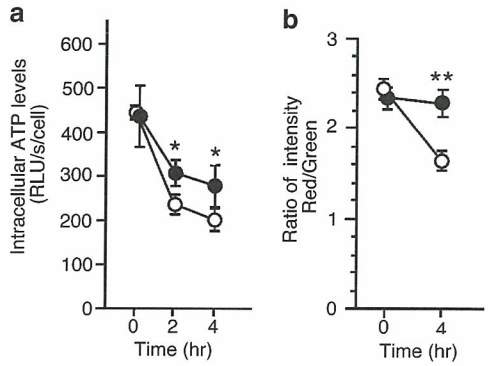

Figure 4 PTD-FNK retains the levels of cellular ATP and the mitochondrial membrane potential in the presence of CCl_4. (**a**) Cells were pre-incubated with 3 nM PTD-FNK (closed circle) or vehicle (open circle) in FBS-free DMEM for 1 h, and continued to culture with 80%-saturated CCl_4 containing 3 nM PTD-FNK or vehicle for the periods indicated. The level of Intracellular ATP per cell was determined using luminescence as described in Materials and methods. Mean values of three independent wells are shown with the S.D.(vertical bars). Statistical analysis was performed using one-way ANOVA: *, $P<0.05$, compared with vehicle. (**b**) Cells were pre-incubated with 3 nM PTD-FNK (closed circle) or vehicle (open circle) in FBS-free DMEM for 1 h and cultured with 80%-saturated CCl_4 in the presence of 3 nM PTD-FNK or vehicle for the periods indicated, followed by being stained with MitoTracker Red and MitoTracker Green FM in fresh DMEM for 30 min. The intensity of fluorescence from each cell was imaged by confocal scanning laser microscopy, and analyzed by using the NIH IMAGE program. Values are expressed as a ratio of the intensity in red divided by that in green of each cell. The mean of the cells examined (PTD-FNK at time 0 and 4 h, 415 and 442 cells, respectively; vehicle at time 0 and 4 h, 425 and 372 cells, respectively) is shown with the S.E. (vertical bars). Statistical analysis was performed using one-way ANOVA: **, $P<0.001$, compared with a vehicle control

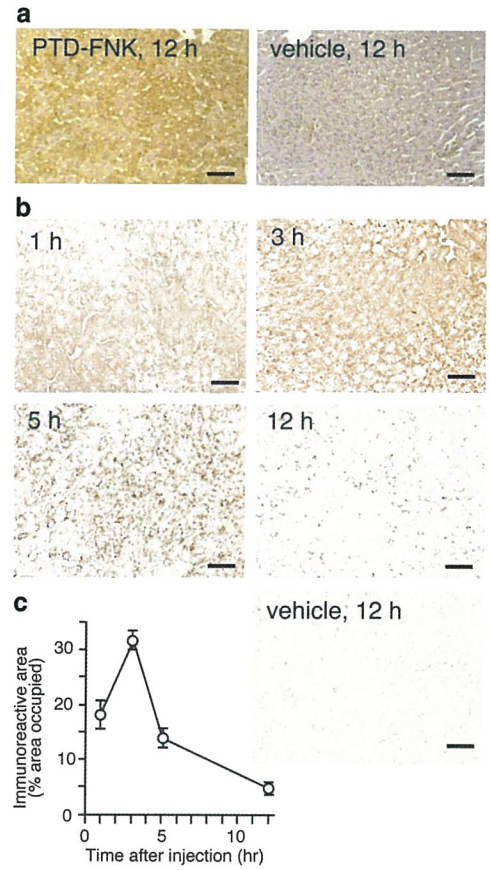

Figure 5 The PTD-FNK protein can be transduced into liver. Male mice (7 weeks old) were injected *i.p.* or *s.c.* with vehicle or PTD-FNK (50 mg/kg). After the indicated periods, the mice were transcardially perfused with cold heparinized physiological saline followed by 4% paraformaldehyde in phosphate-buffered saline (PBS, 0.1 M, pH 7.4), dehydrated and embedded in paraffin. Sections of liver were prepared and subjected to immunohistochemical staining (brown) using anti rat Bcl-x serum. (**a**) *I.p.* injection of PTD-FNK (left) and vehicle (right). Livers were removed at 12 h after *i.p.* These sections were counterstained with hematoxylin (purple) after immunohistochemical staining. Scale bars: 50 μm. (**b**) *S.c.* injection of PTD-FNK. Livers were removed at 1, 3, 5 and 12 h after *s.c.* injection. The immunostained image of liver removed at 12 h after *s.c.* injection of vehicle is also shown. Scale bars: 50 μm. (**c**) Quantitative evaluation of the PTD-FNK remaining in liver after *s.c.* injection. Low-magnification digital images (a half-magnification of (**b**)) of five fields in liver at each time point were analyzed to determine relative areas occupied by Bcl-x immunoreactivity with NIH IMAGE software. The value for liver sections of mice injected with vehicle was used as a background to be subtracted from that for mice injected with the protein. After statistical analysis by one-way ANOVA, the data are shown as means with S.D. (vertical bars). Following the peak at 3 h, PTD-FNK in the liver tissue decreased with a half-span of 3.5 h

nucleus in hepatic cells at both acute and chronic phases (Figures 6c and 7b). A pathologist blindly performed the semi-quantitative histopathological analysis (Table 1).

Pre-injection of PTD-FNK (300 μg/kg) markedly ameliorated this zonal necrosis (Figure 6d and Table 1). Hydropic degeneration of the cytoplasm and pyknosis or loss of nuclei were observed to a small extent in the hepatic cells of mice injected with PTD-FNK, compared to control mice. Serum transaminases, releasing enzymes alanine amino transferase (ALT) and aspartate amino transferase (AST), were measured to evaluate the severity of acute liver injury as a whole (Figure 6a and b). PTD-FNK (300 μg/kg) markedly decreased both activities by two-thirds, compared to vehicle injection. The lower dose of PTD-FNK (75 μg/kg) suppressed the release from liver by one-third compared with the vehicle injection, although the effect was statistically insignificant. The ALT activity decreased at day 2 and was close to a normal level (Figure 7a) on day 3 (data not shown). PTD-Bcl-x_L (300 μg/kg) did not exhibit activity to suppress the release of the enzymes, indicating that PTD-FNK has the stronger activity to protect hepatocytes from cell death induced by CCl_4 *in vivo* as well as *in vitro*.

Post-treatment with PTD-FNK improves acute hepatic injury with a caspase inhibitor

Post-injection of PTD-FNK seemed to only slightly reduce ALT and AST activities in serum (Figure 6a and b), although zonal necrosis was apparently inhibited (Figure 6e and Table 1). The *in vitro* results described above led us to post-inject PTD-FNK with Z-VAD-FMK. The combined post-injection significantly suppressed the elevation of serum ALT and AST, while injection of Z-VAD-FMK alone did not (Figure 6a and b). Histopathological examination also showed that the combined injection profoundly inhibited zonal necrosis (Figure 6f and Table 1). However, no typical apoptotic hepatocyte was found by the TUNEL assay regardless of the injection of PTD-FNK (data not shown).

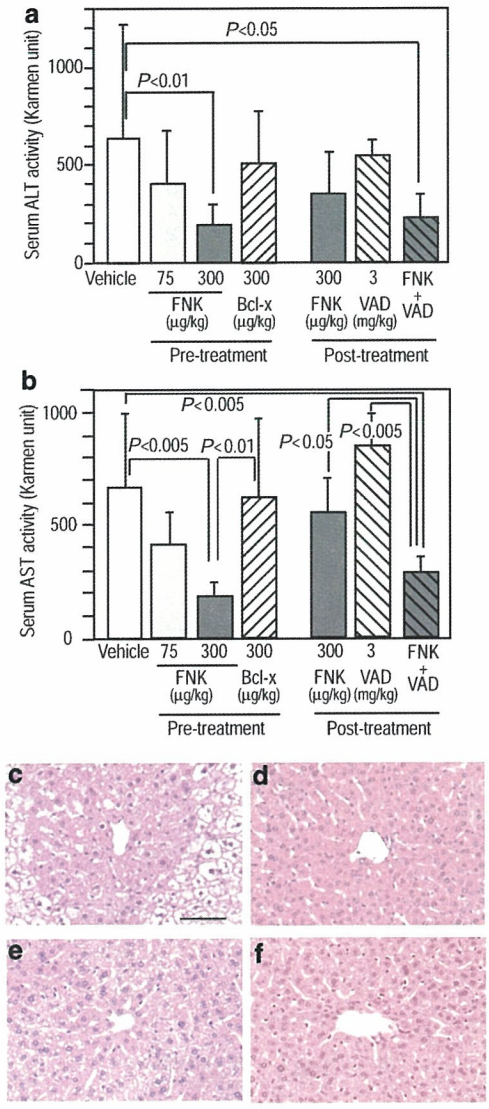

Figure 6 PTD-FNK prevents acute liver injury caused by CCl_4. (**a** and **b**) Animals were *i.p.* injected with vehicle ($n=6$), PTD-FNK (FNK; 75 μg/kg, $n=5$; 300 μg/kg, $n=6$) or PTD-Bcl-x_L (Bcl-x_L; $n=6$) 3 h before the administration of CCl_4 (pre-treatment), or injected with PTD-FNK (FNK; $n=6$), Z-VAD-FMK (VAD; $n=6$) or a combination of PTD-FNK and Z-VAD-FMK (FNK + VAD; $n=6$) 30 min after the administration of CCl_4 (post-treatment). After 20 h, serum (**a**) ALT and (**b**) AST activities were examined and the mean is shown with the S.D. (vertical bars). Statistical analysis was performed using one-way ANOVA. (**c**–**f**) H&E-stained liver tissue sections in the acute phase. Animals pre-injected with (**c**) vehicle or (**d**) PTD-FNK (300 μg/kg), or post-injected with (**e**) PTD-FNK or (**f**) a combination of PTD-FNK and Z-VAD-FMK, were treated with CCl_4. After 20 h, animals were transcardially perfused with 4% paraformaldehyde to prepare paraffin sections of the liver, which were stained with H&E. Scale bar; 100 μm

Thus, post-injection of PTD-FNK with Z-VAD-FMK greatly exhibited the protective effect for acute CCl_4-induced liver injury to the same extent as pre-injection of PTD-FNK.

PTD-FNK prevents chronic liver injury caused by CCl_4

For chronic liver injury, mice were given CCl_4 twice a week for 1 month. On day 4 after the final administration, livers were

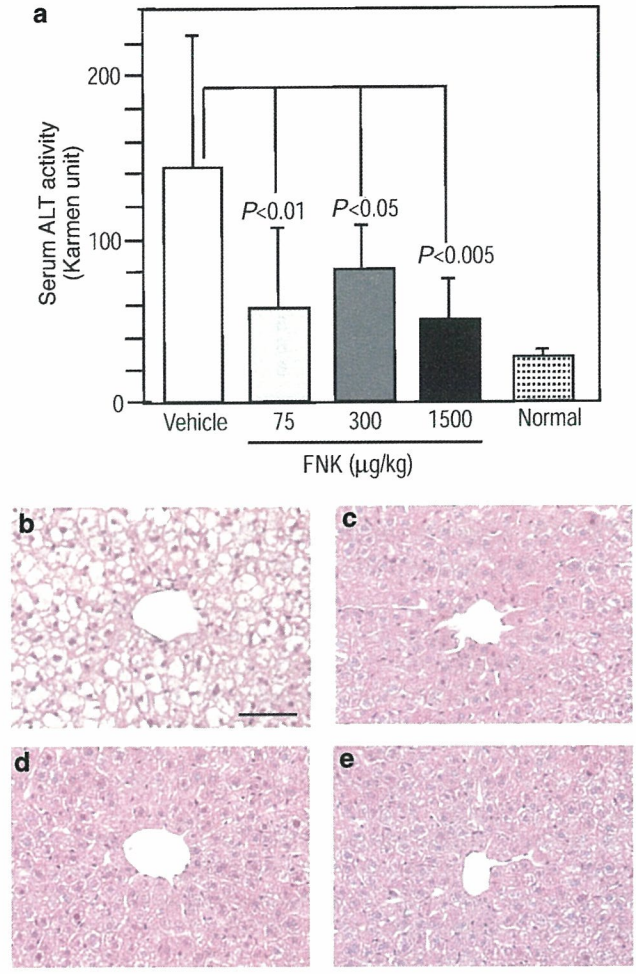

Figure 7 PTD-FNK prevents chronic liver injury caused by CCl_4. (**a**) Animals were *s.c.* injected with vehicle ($n=6$) or PTD-FNK (FNK; 75 μg/kg, $n=5$; 300 μg/kg, $n=6$; 1500 μg/kg, $n=6$) 3 h before the subcutaneous injection of CCl_4, twice a week for a month. On the 4th day after the final administration, serum ALT activity was examined. Normal mice (Normal; $n=6$) without any treatment were also examined. The mean is shown with the S.D. (vertical bars). Statistical analysis was performed using one-way ANOVA. (**b**–**e**) H&E-stained liver tissue sections in the chronic phase. Animals described in (**a**) were sacrificed on the 4th day after the final administration. Livers were taken out to be fixed with 4% paraformaldehyde and embedded in paraffin. The paraffin sections were stained with H&E. (**b**) vehicle, (**c**) 75 μg/kg, (**d**) 300 μg/kg and (**e**) 1500 μg/kg. Scale bar; 100 μm

histopathologically examined and the ALT activity in serum was measured. Histopathological analysis showed that subcutaneous injection of PTD-FNK (75–1500 μg/kg) exhibited marked protective effects on the toxic changes caused by CCl_4, compared with control mice (Table 1). The serum ALT activity of vehicle-injected mice was five to six times higher than the normal level (normal mice without any treatment) (Figure 7a). In mice injected with PTD-FNK, at 75–1500 μg/kg, the activity of serum ALT was markedly lower than that in vehicle-injected mice. Zonal necrosis in the liver of PTD-FNK-treated mice was clearly reduced (Figure 7b–e and Table 1). Taken together, PTD-FNK mitigated chronic liver injury caused by CCl_4.

Table 1 Histopathological analysis of CCl_4-induced liver injury by a semi-quantitative procedure

			Zonal necrosis				Cytoplasm				Nucleus							
							Hydropic degeneration				Pyknosis				Loss			
	PTD-FNK (μg/kg)	Animal no.	–	+	++	+++	–	+	++	+++	–	+	++	+++	–	+	++	+++
Acute	0	4	0	0	0	4	0	0	0	4	0	0	0	4	0	0	4	0
	300 (pre)	4	4	0	0	0	0	0	4	0	0	0	4	0	2	2	0	0
	300 (post)	6	4	2	0	0	0	0	6	0	0	4	2	0	4	2	0	0
	300 with VAD (post)	6	5	1	0	0	0	5	1	0	0	4	2	0	0	6	0	0
Chronic	0	6	0	0	2	4	0	0	2	4	0	0	0	6	0	0	0	6
	75	5	0	2	3	0	0	0	5	0	0	0	5	0	0	4	1	0
	300	6	0	3	3	0	0	0	6	0	0	0	6	0	0	4	2	0
	1500	6	0	3	3	0	0	0	6	0	0	1	5	0	0	5	1	0

–, no pathological findings; +, mild; ++, moderate; +++, severe

PTD-FNK also prevents liver injury induced by ethanol and dexamethasone (DEX)

Next, we examined whether PTD-FNK is applicable to the other models of hepatic injury. EtOH was injected to generate an experimental model of alcoholic hepatic injury. In fact, it caused many lipid deposits (fatty degeneration) to form in the cytoplasm of hepatic cells and also pyknosis in some cells at 12 h (Figure 8a). Injection of PTD-FNK (20 mg/kg, *i.p.*) inhibited the nuclear degeneration but not the fatty degeneration (Figure 8b and Table 2).

A synthetic soluble glucocorticoid, DEX, is an anti-inflammatory drug but affects some hepatotoxicity.[44] The adverse effect by DEX on the liver was evident (Figure 8c). The DEX treatment markedly resulted in the loss of the eosinophilic compartment from the cytoplasm of hepatic cells, which appeared to represent zonal necrosis, but no cholestasis was observed (Figure 8c). Injection of PTD-FNK (5 mg/kg, *i.p.*) clearly ameliorated the zonal necrosis (Figure 8d) and cytoplasmic and nuclear degeneration (Table 2). As DEX induces apoptosis at high doses, liver sections were stained using the TUNEL assay. In vehicle-injected liver sections, DEX induced many TUNEL-positive cells (Figure 8e), while PTD-FNK reduced the number of TUNEL-positive cells by half, indicating that PTD-FNK prevents DEX-induced hepatic injury. Thus, PTD-FNK seemed to protect hepatocytes against various injuries regardless of apoptosis or necrosis.

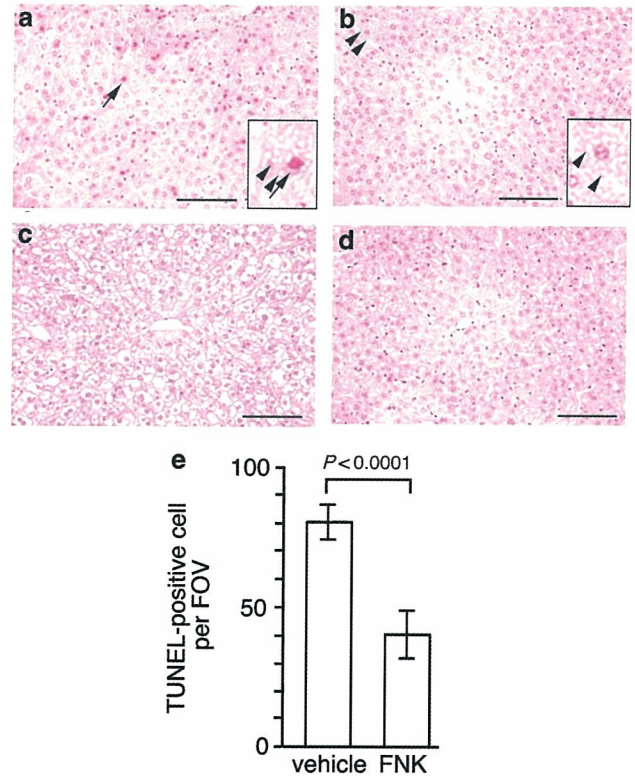

Figure 8 PTD-FNK prevents liver injury induced by ethanol or dexamethasone. Mice were intraperitoneally injected with vehicle or PTD-FNK 3 h before the administration of drugs. (**a** and **b**) Ethanol-induced injury. Mice pre-injected with vehicle (**a**) or PTD-FNK (20 mg/kg) (**b**) were treated with ethanol. After 12 h, animals were transcardially perfused and liver sections were stained with H&E. Arrows and arrowheads indicate pyknosis and lipid deposits, respectively, and have been enlarged in the insets. (**c** and **d**) DEX-induced injury. Mice pre-injected with vehicle (**c**) and PTD-FNK (5 mg/kg) (**d**) were treated with DEX. After 24 h, animals were transcardially perfused and liver sections were stained with H&E. Scale bars: (**a–d**), 100 μm. (**e**) The number of TUNEL-positive cells per high-powered field of view (FOV) in the liver sections prepared from the DEX-treated mice injected with vehicle or PTD-FNK (FNK). TUNEL-positive cells were counted in five non-overlapping fields per slide from each liver ($n=20$ microscopic fields). The vertical bars show the S.D. and statistical analysis was performed using the Student's *t*-test

Discussion

We addressed the question of whether FNK can protect cells from necrotic death via protein transduction technology using the PTD of HIV/Tat.

Under *in vitro* experimental conditions, the addition of 80%-saturated CCl_4/DMEM lacking serum caused death of HepG2 cells with no activation of caspase-3/caspase-3-like activity, no nuclear fragmentation, no ladder formation of DNA in 8 h, and no binding to Annexin V in the early stage. Detection of a 50 kDa fragment derived from PARP-1 in CCl_4-treated cells is strong evidence for necrosis, because the apoptotic PARP-1 fragment of 85 kDa induced with TNFα/CHX is distinct from the 50 kDa fragment[38,39] (Figure 1d). These results clearly

Table 2 Histopathological analysis of ethanol (EtOH)- or dexamethasone (DEX)-induced liver injury by a semi-quantitative procedure

			Zonal necrosis				Cytoplasm								Nucleus							
							Hydropic degeneration				Fatty degeneration				Pyknosis				Loss			
	PTD-FNK (mg/kg)	Animal no.	–	+	++	+++	–	+	++	+++	–	+	++	+++	–	+	++	+++	–	+	++	+++
EtOH	0	4	4	0	0	0	4	0	0	0	0	0	4	0	0	4	0	0	4	0	0	0
	20	4	4	0	0	0	4	0	0	0	0	0	4	0	4	0	0	0	4	0	0	0
DEX	0	4	0	0	0	4	0	0	1	3	4	0	0	0	0	0	1	3	0	0	4	0
	5	4	0	4	0	0	0	0	4	0	4	0	0	0	2	2	0	0	4	0	0	0

–, no pathological findings; +, mild; ++, moderate; +++, severe

indicated that a majority of HepG2 cells exposed to CCl_4 died in a necrotic manner, with a good agreement with previous results.[45] The results of the application of PTD-FNK and PTD-Bcl-x_L have two implications. The first is that PTD-FNK significantly protected the cells from necrotic death induced by CCl_4, compared with PTD-Bcl-x_L. The second is that PTD-FNK clearly increased the apoptotic population among cells treated with CCl_4. The result may imply that the necrotic pathway activated by CCl_4 uses apoptotic mediator(s) in some steps, as discussed below. In fact, PTD-FNK with Z-VAD-FMK protected around 60% of cells from CCl_4-induced necrotic death. A plausible explanation for these results is that treatment with PTD-FNK or -Bcl-x_L caused a switch from a necrotic to apoptotic pathway and that, in turn, Z-VAD-FMK protects these cells from the apoptosis. On the other hand, a small population among the HepG2 cells treated with CCl_4 had fragmented nuclei even in the absence of PTD-FNK (Figure 3a). However, the apoptotic morphology seems to be caused by the withdrawal of serum but not by the addition of CCl_4 because the Annexin-V-positive and PI-negative population was equivalent between cells treated and untreated with CCl_4 (Figure 3d). In double-positive cells with Annexin V and PI, Annexin V may have entered into cells and bound to phosphatidylserine remaining at inner side of the plasma membrane.[46]

Apoptosis has been distinguished from necrosis by morphological and biochemical characteristics including activation of caspases. Recent evidences showed that some biochemical and morphological characteristics of both modes of cell death can be found in the same cell.[1] It is also argued that physiological cell deaths exist that do not appear to be typical apoptosis or dependent on the caspase activation.[47] Appearance of these complex death forms can be explained by interception of active cellular death processes by, for example, oxygen-radical scavengers and inhibition of caspase or PARP.[48–50] Our results support the hypothesis that necrosis and typical apoptosis are two extremes of a spectrum of death programs varying with the strength of the death stimulus.[1] It is noted that mitochondria play an important role in necrosis as well as apoptosis.[1,47] As PTD-FNK was shown to localize in the mitochondria,[17,18] further studies on the function of PTD-FNK would provide insight into the correlation between apoptosis and necrosis. Since FNK exhibited clearer results than Bcl-x_L, FNK will be useful for investigating this issue in future.

How does PTD-FNK protect cells from CCl_4-induced necrosis? The hepatic cell death caused by CCl_4 is clearly due to necrosis (oncosis), although a careful study demonstrated that a small population of hepatocytes undergoes apoptosis in acute CCl_4-induced liver injury.[51] It is generally accepted that CCl_4 is metabolized to the trichloromethyl free radical by the monooxidase system of the ER, where cytochrome P450, mainly isozyme CYP2E1, is thought to play an important role in the pathogenesis.[52] Following production of toxic reactive intermediates, autocatalytic lipid peroxidation is suggested to damage cellular macromolecules, but the cellular mechanisms responsible for CCl_4-induced hepatic cell death are poorly understood.[53] The HepG2 cells used here do not express significant amounts of the enzyme.[54] Since PTD-FNK retained the intracellular level of ATP and mitochondrial membrane potential, the protein seems to preserve functional mitochondria to protect cells.

Another evidence is emerging that calcium ions are involved in the CCl_4-induced cytotoxicity.[53–56] CCl_4 affects intracellular Ca^{2+} content and seems to inhibit differently calcium transport systems on the cytoplasmic, mitochondrial and ER membranes.[56] Calcium ions activate lytic enzymes such as phospholipase A2 that may cause disintegrity of the organelle membrane, including the cytoplasmic membrane.[57] Thus, cytoplasmic Ca^{2+} seems generally to play a key role in necrosis. Interestingly, many studies indicate alterations in the intracellular Ca^{2+} homeostasis to control apoptosis.[58] Bcl-2 inhibits a release of Ca^{2+} from the ER induced by the pro-apoptotic Bcl-2 family members Bax or Bak.[59] PTD-FNK likely inhibits the disruption of Ca^{2+} homeostasis induced by CCl_4 because PTD-FNK affects the cytosolic movement of Ca^{2+} and protects neuronal cells from glutamate excitotoxicity.[18]

PTD-FNK injected into mice was successfully delivered to the liver and prevented the acute and chronic death of hepatocytes caused by CCl_4. On post-injection of PTD-FNK, an injection of Z-VAD-FMK significantly reduced the acute liver injury, as expected from the *in vitro* studies, indicating that the therapeutic window for combined injections extends after the administration of CCl_4. PTD-FNK injection also prevented alchohol- and DEX-induced liver injury. Ethanol was recently shown to generate free radicals in mice and rats,[60,61] increasing the frequency of DNA-strand breaks in the liver.[60] PTD-FNK probably inhibited pyknosis caused by free radicals, while it did not affect fatty accumulation as a

product of the EtOH metabolism. DEX treatment decreases the glutathione concentration in liver[44] and, at a high dose, causes reversible hepatomegaly with hepatopathy.[62] It is also reported that DEX co-administered with methotrexate induced liver damage during a treatment for brain tumor.[63]

This study strongly suggests that PTD-FNK is a potent therapeutic protein to prevent necrotic and apoptotic cell death for emergency care and will allow the development of a novel therapy to prevent cell death by preventing necrosis.

Materials and Methods

Preparation of PTD-FNK

PTD-FNK and PTD-Bcl-x_L were prepared as described previously.[18] In brief, the proteins were recovered as inclusion bodies from *Escherichia coli* cells after treatment with isopropyl 1-thio-β-D-galactoside. The proteins were solubilized in a buffer (7 M urea, 2% SDS, 1 mM DTT, 62.5 mM Tris-HCl (pH 6.8) and 150 mM NaCl), and then subjected to SDS-PAGE to remove contaminating proteins and endotoxin. The gel was treated with 1 M KCl and the transparent band corresponding to PTD-FNK or PTD-Bcl-x_L was cut out. The proteins were electrophoretically extracted from the gel slice in an extraction buffer (25 mM Tris, 0.2 M glycine and 0.1% SDS) for *in vitro* and *in vivo* experiments. The extraction buffer was used as a control (vehicle). The concentration of PTD-FNK or PTD-Bcl-x_L extracted ranged from 1 to 2.5 mg/ml.

Chemicals

CCl_4 and STS were purchased from Wako Pure Chemical Industries Ltd (Osaka, Japan) and Sigma (Sigma-Aldrich Japan, Tokyo, Japan), respectively. Caspase inhibitor I, Z-VAD-FMK, was obtained from Calbiochem (Merck Japan Ltd, Tokyo, Japan). Human recombinant TNFα was purchased from Sigma. Olive oil (Sigma) was used as a solvent of CCl_4 for injection.

Cell culture and drug-inducing cell death

The human hepatoma cell line HepG2 was cultured in DMEM (Life Technologies, Invitrogen, Tokyo, Japan) containing 10% fetal bovine serum (FBS). Cells were plated at 5×10^3 (or 1×10^4) cells/well in a 48-well (or 24-well) IWAKI EZView™ culture plate (Asahi Techno Glass, Tokyo, Japan), which had been coated with collagen type I (Cellmatrix I-P, Nitta Gelatin Inc., Osaka, Japan). After 2 days, the cells were treated with drugs. For CCl_4 treatment, cells were washed with FBS-free DMEM twice and treated with 80%-saturated CCl_4 in DMEM without FBS. FBS-free DMEM was brought to 80% CCl_4 saturation by adding CCl_4-saturated DMEM, where the CCl_4-saturated DMEM was prepared as follows: excess amounts of CCl_4 were added to FBS-free DMEM in a glass bottle and incubated for 15–18 h at 37°C. Hoechst 33342 and PI, 5 μM each, were added to the cells after various incubation periods. To detect cells in the early stage of apoptosis, the cells were stained with Annexin-V-FLUOS (green dye) and PI using a Annexin-V-FLUOS Staining Kit (Roche Diagnostics GmbH, Mannheim, Germany). Annexin-V-positive and PI-negative cells were judged as apoptotic ones. For STS treatment, cells in DMEM with FBS were treated with 10 μM STS. For TNFα treatment, cells in DMEM with FBS were pretreated with CHX (10 μg/ml) for 30 min, and then TNFα was added at the concentration of 1 and 10 ng/ml.

Caspase-3/caspase-3-like activity assay and DNA fragmentation

HepG2 (1×10^5) cells were plated in a 60-mm glass dish coated with collagen type I. After 2 days, the cells were treated with CCl_4 or STS for various periods as mentioned above. Harvested cells were lysed and a caspase fluorescence assay was performed using Ac-DEVD-AMC (*N*-acetyl-Asp-Glu-Val-Asp-7-amino-4-methylcoumarin), with or without the inhibitor Ac-DEVD-CHO (*N*-acetyl-Asp-Glu-Val-Asp-CHO (aldehyde)), and a Caspase Fluorescent (AMC) Substrate/Inhibitor QuantiPack™ (BIOMOL Research Laboratories Inc., PA, USA). Protein concentration was determined with the BCA Protein Assay (Pierce, IL, USA) using BSA as a standard. For the detection of DNA ladders, harvested cells were lysed with 0.5% Triton X-100, and then centrifuged to remove intact nuclei as reported previously.[64] After digestion with proteinase K and RNase A, fragmented DNA was precipitated with 2-propanol. DNA from 0.6×10^5 cells was subjected to electrophoresis on a 2% agarose gel, stained with SYBR Green (Molecular Probes Inc., OR, USA). With this method, DNA from intact nuclei was excluded, and thus the intact DNA did not disturb the pattern of electrophoresis.

Western blot analysis

Cells were harvested and washed. The total protein was solubilized in the presence of 2% SDS by sonication. Protein concentration was determined with the BCA Protein Assay (Pierce) using BSA as a standard. After separated on a SDS-polyacrylamide gradient (4–20%) gel, the proteins were transferred onto a PolyScreen polyvinylidiene fluoride membrane (NEN Life Science Product Inc., Boston, MA, USA). The membrane was treated with anti-human PARP (clone 7D3-6; BD Biosciences Pharmingen, San Diego CA, USA). The intact form and digested products of PARP-1 were visualized with a fluoro bioimaging analyzer FLA-2000 (Fuji Photo Film, Tokyo) using the AttoPhos kit (Roche Diagnostics K.K., Tokyo).

ATP measurement

Cells were plated at 5×10^3 cells/well in a 48-well IWAKI EZView™ culture plate coated with collagen type I. After 2 days, the cells were treated with 80%-saturated CCl_4/DMEM for 0 to 4 h. After the CCl_4/DMEM solution was removed, 100 μl of DMEM without FBS was added to the wells and ATP levels were determined using a 'Cellno' ATP Assay Kit Type N (TOYO B-Net Co., Ltd, Tokyo) as per the manufacturer's instructions. Briefly, 100 μl of the lysis/assay solution provided by the manufacturer was added to the wells. After shaking for 1 min and incubating for 10 min at 23°C, luminescence of an aliquot of the solution was measured in a luminometer, Lumat LB9507 (Berthold Technologies, Berthold Japan Co., Ltd, Tokyo).

Membrane potential measurement

Cells were plated at 1×10^4 cells/well in a 24-well IWAKI EZView™ culture plate coated with collagen type I. After 2 days, the cells were treated with 80%-saturated CCl_4/DMEM for 0 and 4 h. The CCl_4 solution was removed and DMEM containing 100 nM MitoTracker Red CMXRos (Molecular Probes) and 200 nM MitoTracker Green FM (Molecular Probes) was added. After 30-min incubation, fluorescence was imaged by confocal scanning laser microscopy (Fluoview FV/300; Olympus, Tokyo). The Images were analyzed by using the NIH IMAGE program to obtain a ratio of mean intensity in red divided by mean intensity in green of each cell, where the ratio reflects mitochondrial membrane potential of each cell.

Drug-induced liver injury

Male, 4- to 5-week-old C57BL/6N mice (Seac Yoshitomi Ltd, Yoshitomi-cho, Fukuoka, Japan) were used. For acute liver injury induced by CCl_4, mice were *i.p.* injected with CCl_4 (25 mg/kg). After 20 h, blood was obtained for biochemical examinations and mice were perfused transcardially and livers fixed with 4% paraformaldehyde in 0.1 M phosphate buffer (pH 7.4), dehydrated and embedded in paraffin. For acute liver injury induced by ethanol and DEX (Sigma), ethanol (5 g/kg) or DEX (25 mg/kg) was *i.p.* administered. After specified periods, mice were transcardially perfused and livers fixed with 4% paraformaldehyde, dehydrated and embedded in paraffin as described above. For chronic liver injury caused by CCl_4, mice were subcutaneously injected with vehicle or PTD-FNK 3 h before the subcutaneous injection of CCl_4 (25 mg/kg), twice a week for a month. On the 4th day after the final administration, blood was obtained for biochemical examinations and mice were killed. Livers were removed for fixation with 4% paraformaldehyde in 0.1 M phosphate buffer (pH 7.4), dehydrated and embedded in paraffin. Tissues were sectioned (4 μm), and stained with H&E for histopathological analysis. Activities of serum AST and ALT were evaluated using a Transaminase CII Testwako kit (Wako Pure Chemical Industries Ltd). Animal protocols were approved by the Animal Care and Use Committee of Nippon Medical School.

Immunohistochemical staining

The delivery of PTD-FNK into the liver was examined according to the manufacturer's protocol using a Vectastain ABC elite kit (Vector Laboratories, Burlingame, CA, USA) coupled to a diaminobenzidine (DAB) reaction. Rabbit polyclonal anti rat Bcl-x serum (diluted 1 : 250 at 4°C overnight) was used as a primary antibody. In addition, phosphate-buffered saline (PBS) was utilized instead of primary antibody and/or ABC reagent as a negative control.

Terminal deoxynucleotidyl transferase-mediated dUTP nick-end labeling (TUNEL)

Separate sections were used for TUNEL staining using an ApopTag peroxidase *In situ* Apoptosis Detection Kit (Intergen Company, Purchase, New York, USA), and visualized with DAB. For negative controls, terminal deoxynucleotidyl transferase was omitted. In each section, TUNEL-positive cells were counted in five non-overlapping microscopic fields ($\times$ 100 magnification).

References

1. Proskuryakov SY, Konoplyannikov AG and Gabai VL (2003) Necrosis: a specific form of programmed cell death? Exp. Cell Res. 283: 1–16
2. Nathan C (2002) Points of control in inflammation. Nature 420: 846–852
3. Roos KL (1990) Dexamethasone and nonsteroidal anti-inflammatory agents in the treatment of bacterial meningitis. Clin. Ther. 12: 290–296
4. Tracey KJ (2002) The inflammatory reflex. Nature 420: 853–859
5. Palladino MA, Bahjat FR, Theodorakis EA and Moldawer LL (2003) Anti-TNF-alpha therapies: the next generation. Nat. Rev. Drug Discov. 2: 736–746
6. Boise LH, Gonzalez-Garcia M, Postema CE, Ding L, Lindsten T, Turka LA, Mao X, Nunez G and Thompson CB (1993) *bcl-x*, a *bcl-2*-related gene that functions as a dominant regulator of apoptotic cell death. Cell 74: 597–608
7. Minn AJ, Rudin CM, Boise LH and Thompson CB (1995) Expression of Bcl-x_L can confer a multidrug resistance phenotype. Blood 86: 1903–1910
8. Yang J, Liu X, Bhalla K, Kim CN, Ibrado AM, Cai J, Peng TI, Jones DP and Wang X (1997) Prevention of apoptosis by Bcl-2: release of cytochrome *c* from mitochondria blocked. Science 275: 1129–1132
9. Jäättelä M, Benedict M, Tewari M, Shayman JA and Dixit VM (1995) Bcl-x and Bcl-2 inhibit TNF and Fas-induced apoptosis and activation of phospholipase A2 in breast carcinoma cells. Oncogene 10: 2297–2305
10. Fukunaga-Johnson N, Ryan JJ, Wicha M, Nunez G and Clarke MF (1995) Bcl-2 protects murine erythroleukemia cells from p53-dependent and -independent radiation-induced cell death. Carcinogenesis 16: 1761–1767
11. Cory S, Huang DC and Adams JM (2003) The Bcl-2 family: roles in cell survival and oncogenesis. Oncogene 22: 8590–8607
12. Tsujimoto Y, Shimizu S, Eguchi Y, Kamiike W and Matsuda H (1997) Bcl-2 and Bcl-x_L block apoptosis as well as necrosis: possible involvement of common mediators in apoptotic and necrotic signal transduction pathways. Leukemia 11: 380–382
13. Single B, Leist M and Nicotera P (2001) Differential effects of *bcl-2* on cell death triggered under ATP-depleting conditions. Exp. Cell Res. 262: 8–16
14. Asoh S, Ohtsu T and Ohta S (2000) The super anti-apoptotic factor Bcl-xFM constructed by disturbing intramolecular polar interactions in rat Bcl-x_L. J. Biol. Chem. 275: 37240–37245
15. Nagahara H, Vocero-Akbani AM, Snyder EL, Ho A, Latham DG, Lissy NA, Becker-Hapak M, Ezhevsky SA and Dowdy SF (1998) Transduction of full-length TAT fusion proteins into mammalian cells: TAT-$p27^{Kip1}$ induces cell migration. Nat. Med. 4: 1449–1452
16. Schwarze SR, Ho A, Vocero-Akbani A and Dowdy SF (1999) *In vivo* protein transduction: delivery of a biologically active protein into the mouse. Science 285: 1569–1572
17. Ozaki D, Sudo K, Asoh S, Yamagata K, Ito H and Ohta S (2004) Transduction of anti-apoptotic proteins into chondrocytes in cartilage slice culture. Biochem. Biophys. Res. Commun. 313: 522–527
18. Asoh S, Ohsawa I, Mori T, Katsura K, Hiraide T, Katayama Y, Kimura M, Ozaki D, Yamagata K and Ohta S (2002) Protection against ischemic brain injury by protein therapeutics. Proc. Natl. Acad. Sci. USA 99: 17107–17112
19. Graham SH and Chen J (2001) Programmed cell death in cerebral ischemia. J. Cereb. Blood Flow Metab. 21: 99–109
20. Valencia A and Moran J (2004) Reactive oxygen species induce different cell death mechanisms in cultured neurons. Free Radic. Biol. Med. 36: 1112–1125
21. Lin Y, Choksi S, Shen HM, Yang QF, Hur GM, Kim YS, Tran JH, Nedospasov SA and Liu ZG (2004) Tumor necrosis factor-induced nonapoptotic cell death requires receptor-interacting protein-mediated cellular reactive oxygen species accumulation. J. Biol. Chem. 279: 10822–10828
22. Higuchi M, Honda T, Proske RJ and Yeh ET (1998) Regulation of reactive oxygen species-induced apoptosis and necrosis by caspase 3-like proteases. Oncogene 17: 2753–2760
23. Lee WT, Itoh T and Pleasure D (2002) Acute and chronic alterations in calcium homeostasis in 3-nitropropionic acid-treated human NT2-N neurons. Neuroscience 113: 699–708
24. Zhu LP, Yu XD, Ling S, Brown RA and Kuo TH (2000) Mitochondrial Ca^{2+} homeostasis in the regulation of apoptotic and necrotic cell deaths. Cell Calcium 28: 107–117
25. Gwag BJ, Canzoniero LM, Sensi SL, Demaro JA, Koh JY, Goldberg MP, Jacquin M and Choi DW (1999) Calcium ionophores can induce either apoptosis or necrosis in cultured cortical neurons. Neuroscience 90: 1339–1348
26. Pritchard DJ and Butler WH (1989) Apoptosis – the mechanism of cell death in dimethylnitrosamine-induced hepatotoxicity. J. Pathol. 158: 253–260
27. Fukuda K, Kojiro M and Chiu JF (1993) Demonstration of extensive chromatin cleavage in transplanted Morris hepatoma 7777 tissue: apoptosis or necrosis? Am. J. Pathol. 142: 935–946
28. Grasl-Kraupp B, Ruttkay-Nedecky B, Koudelka H, Bukowska K, Bursch W and Schulte-Hermann R (1995) *In situ* detection of fragmented DNA (TUNEL assay) fails to discriminate among apoptosis, necrosis, and autolytic cell death: a cautionary note. Hepatology 21: 1465–1468
29. Columbano A, Endoh T, Denda A, Noguchi O, Nakae D, Hasegawa K, Ledda-Columbano GM, Zedda AI and Konishi Y (1996) Effects of cell proliferation and cell death (apoptosis and necrosis) on the early stages of rat hepatocarcinogenesis. Carcinogenesis 17: 395–400
30. Noguchi T, Fong KL, Lai EK, Alexander SS, King MM, Olson L, Poyer JL and McCay PB (1982) Specificity of a phenobarbital-induced cytochrome P-450 for

metabolism of carbon tetrachloride to the trichloromethyl radical. Biochem. Pharmacol. 31: 615–624
31. Ahr HJ, King LJ, Nastainczyk W and Ullrich V (1982) The mechanism of reductive dehalogenation of halothane by liver cytochrome P450. Biochem. Pharmacol. 31: 383–390
32. Nastainczyk W, Ahr HJ and Ullrich V (1982) The reductive metabolism of halogenated alkanes by liver microsomal cytochrome P450. Biochem. Pharmacol. 31: 391–396
33. Poyer JL, McCay PB, Lai EK, Janzen EG and Davis ER (1980) Confirmation of assignment of the trichloromethyl radical spin adduct detected by spin trapping during ^{13}C-carbon tetrachloride metabolism *in vitro* and *in vivo*. Biochem. Biophys. Res. Commun. 94: 1154–1160
34. Lai EK, McCay PB, Noguchi T and Fong KL (1979) *In vivo* spin-trapping of trichloromethyl radicals formed from CCl_4. Biochem. Pharmacol. 28: 2231–2235
35. Berger ML, Bhatt H, Combes B and Estabrook RW (1986) CCl_4-induced toxicity in isolated hepatocytes: the importance of direct solvent injury. Hepatology 6: 36–45
36. Jones BE, Lo CR, Liu H, Srinivasan A, Streetz K, Valentino KL and Czaja MJ (2000) Hepatocytes sensitized to tumor necrosis factor-alpha cytotoxicity undergo apoptosis through caspase-dependent and caspase-independent pathways. J. Biol. Chem. 275: 705–712
37. Bai J and Cederbaum AI (2000) Overexpression of catalase in the mitochondrial or cytosolic compartment increases sensitivity of HepG2 cells to tumor necrosis factor-alpha-induced apoptosis. J. Biol. Chem. 275: 19241–19249
38. Gobeil S, Boucher CC, Nadeau D and Poirier GG (2001) Characterization of the necrotic cleavage of poly(ADP-ribose) polymerase (PARP-1): implication of lysosomal proteases. Cell Death Differ. 8: 588–594
39. Shah GM, Shah RG and Poirier GG (1996) Different cleavage pattern for poly(ADP-ribose) polymerase during necrosis and apoptosis in HL-60 cells. Biochem. Biophys. Res. Commun. 229: 838–844
40. Aikin R, Rosenberg L, Paraskevas S and Maysinger D (2004) Inhibition of caspase-mediated PARP-1 cleavage results in increased necrosis in isolated islets of Langerhans. J. Mol. Med. 82: 389–397
41. Horn TL, O'Brien TD, Schook LB and Rutherford MS (2000) Acute hepatotoxicant exposure induces TNFR-mediated hepatic injury and cytokine/apoptotic gene expression. Toxicol. Sci. 54: 262–273
42. Morio LA, Chiu H, Sprowles KA, Zhou P, Heck DE, Gordon MK and Laskin DL (2001) Distinct roles of tumor necrosis factor-alpha and nitric oxide in acute liver injury induced by carbon tetrachloride in mice. Toxicol. Appl. Pharmacol. 172: 44–51
43. Simeonova PP, Gallucci RM, Hulderman T, Wilson R, Kommineni C, Rao M and Luster MI (2001) The role of tumor necrosis factor-alpha in liver toxicity, inflammation, and fibrosis induced by carbon tetrachloride. Toxicol. Appl. Pharmacol. 177: 112–120
44. Madhu C, Maziasz T and Klaassen CD (1992) Effect of pregnenolone-16 alpha-carbonitrile and dexamethasone on acetaminophen-induced hepatotoxicity in mice. Toxicol. Appl. Pharmacol. 115: 191–198
45. Jäättelä M and Tschopp J (2003) Caspase-independent cell death in T lymphocytes. Nat. Immunol. 4: 416–423
46. Vermes I, Haanen C, Steffens-Nakken H and Reutelingsperger C (1995) A novel assay for apoptosis. Flow cytometric detection of phosphatidylserine expression on early apoptotic cells using fluorescein labelled Annexin V. J. Immunol. Methods. 184: 39–51
47. Lockshin RA and Zakeri Z (2004) Caspase-independent cell death? Oncogene 23: 2766–2773
48. Vercammen D, Brouckaert G, Denecker G, Van de Craen M, Declercq W, Fiers W and Vandenabeele P (1998) Dual signaling of the Fas receptor: initiation of both apoptotic and necrotic cell death pathways. J. Exp. Med. 188: 919–930
49. Vercammen D, Beyaert R, Denecker G, Goossens V, Van Loo G, Declercq W, Grooten J, Fiers W and Vandenabeele P (1998) Inhibition of caspases increases the sensitivity of L929 cells to necrosis mediated by tumor necrosis factor. J. Exp. Med. 187: 1477–1485
50. Ha HC and Snyder SH (1999) Poly(ADP-ribose) polymerase is a mediator of necrotic cell death by ATP depletion. Proc. Natl. Acad. Sci. USA 96: 13978–13982
51. Shi J, Aisaki K, Ikawa Y and Wake K (1998) Evidence of hepatocyte apoptosis in rat liver after the administration of carbon tetrachloride. Am. J. Pathol. 153: 515–525
52. Raucy JL, Kraner JC and Lasker JM (1993) Bioactivation of halogenated hydrocarbons by cytochrome P4502E1. Crit. Rev. Toxicol. 23: 1–20
53. Recknagel RO, Glende Jr EA, Dolak JA and Waller RL (1989) Mechanisms of carbon tetrachloride toxicity. Pharmacol. Ther. 43: 139–154
54. Cederbaum AI, Wu D, Mari M and Bai J (2001) CYP2E1-dependent toxicity and oxidative stress in HepG2 cells. Free Radic. Biol. Med. 31: 1539–1543
55. Costa AK, Schieble TM, Heffel DF and Trudell JR (1987) Toxicity of calcium ionophore A23187 in monolayers of hypoxic hepatocytes. Toxicol. Appl. Pharmacol. 87: 43–47
56. Hemmings SJ, Pulga VB, Tran ST and Uwiera RR (2002) Differential inhibitory effects of carbon tetrachloride on the hepatic plasma membrane, mitochondrial and endoplasmic reticular calcium transport systems: implications to hepatotoxicity. Cell Biochem. Funct. 20: 47–59
57. Glende Jr EA and Pushpendran CK (1986) Activation of phospholipase A2 by carbon tetrachloride in isolated rat hepatocytes. Biochem. Pharmacol. 35: 3301–3307
58. Breckenridge DG, Germain M, Mathai JP, Nguyen M and Shore GC (2003) Regulation of apoptosis by endoplasmic reticulum pathways. Oncogene 22: 8608–8618
59. Nutt LK, Pataer A, Pahler J, Fang B, Roth JA, McConkey DJ and Swisher SG (2002) Bax and Bak promote apoptosis by modulating endoplasmic reticular and mitochondrial Ca^{2+} stores. J. Biol. Chem. 277: 9219–9225
60. Navasumrit P, Ward TH, Dodd NJ and O'Connor PJ (2000) Ethanol-induced free radicals and hepatic DNA strand breaks are prevented *in vivo* by antioxidants: effects of acute and chronic ethanol exposure. Carcinogenesis 21: 93–99
61. Kono H, Rusyn I, Yin M, Gabele E, Yamashina S, Dikalova A, Kadiiska MB, Connor HD, Mason RP, Segal BH, Bradford BU, Holland SM and Thurman RG (2000) NADPH oxidase-derived free radicals are key oxidants in alcohol-induced liver disease. J. Clin. Invest. 106: 867–872
62. Verrips A, Rotteveel JJ and Lippens R (1998) Dexamethasone-induced hepatomegaly in three children. Pediatr. Neurol. 19: 388–391
63. Wolff JE, Hauch H, Kuhl J, Egeler RM and Jurgens H (1998) Dexamethasone increases hepatotoxicity of MTX in children with brain tumors. Anticancer Res. 18: 2895–2899
64. Asoh S, Mori T, Hayashi J and Ohta S (1996) Expression of the apoptosis-mediator Fas is enhanced by dysfunctional mitochondria. J. Biochem. (Tokyo) 120: 600–607